

1 **If a Tree Falls in the Forest Does it Make a Splash? Forest Restoration in the Central**
2 **Sierra Nevada Provides a Robust Hydrological Hedge Against Droughts**

3 **E. N. Boardman¹, Z. Duan², M. S. Wigmosta², S. W. Flake³, M. R. Sloggy⁴, J. Tarricone^{1,5,6}, A. A.**
4 **Harpold^{1,7}**

5 ¹Graduate Program of Hydrologic Sciences, University of Nevada, Reno, Reno, NV, USA

6 ²Pacific Northwest National Laboratory, Richland, WA, USA

7 ³Department of Forestry and Environmental Resources, North Carolina State University,
8 Raleigh, NC, USA

9 ⁴Pacific Southwest Research Station, U.S. Forest Service, Riverside, CA, USA

10 ⁵Hydrological Sciences Laboratory, NASA Goddard Spaceflight Center, Greenbelt, MD, USA

11 ⁶NASA Postdoctoral Program, NASA Goddard Space Flight Center, Greenbelt, MD, USA

12 ⁷Department of Natural Resources and Environmental Science, University of Nevada, Reno,
13 Reno, NV, USA

14
15 Corresponding author: Elijah N. Boardman (eli.boardman@mountainhydrology.com)

16
17 **Key Points:**

- 18 • Restoring historic forest disturbance return intervals can increase water yield by 8-14%
19 during dry years in the central Sierra Nevada.
- 20 • Understory largely compensates for reduced overstory transpiration, so 73% of
21 streamflow gains are attributable to reduced interception.
- 22 • Thinner forests can increase headwaters peak flows, but climate uncertainty
23 overwhelms this effect at the reservoir scale.
24

25 **Abstract**

26 Forest thinning and prescribed fire are expected to improve the climate resilience and water
27 security of forests in the western U.S., but few studies have directly modeled the hydrological
28 effects of multi-decadal landscape-scale forest restoration. By updating a distributed process-
29 based hydrological model (DHSVM) with vegetation maps from a distributed forest ecosystem
30 model (LANDIS-II), we simulate the water resource impacts of forest management scenarios
31 targeting partial or full restoration of the historic disturbance return interval in the central
32 Sierra Nevada mountains. In a fully restored disturbance regime, the models predict additional
33 reservoir inflow of 4-9% total and 8-14% in dry years. At sub-watershed scales (10-100 km²),
34 thinning dense forests can increase streamflow generation by >20% in dry years. In a thinner
35 forest, increased understory transpiration largely compensates for decreased overstory
36 transpiration. Consequentially, 73% of streamflow gains are attributable to decreased overstory
37 interception loss. Thinner forests can increase headwater peak flows, but reservoir-scale peak
38 flows are almost exclusively influenced by climate projections. Uncertainty in the future
39 precipitation volume causes high uncertainty in the future water yield, but the additional
40 volume of water attributable to forest restoration is about five times less sensitive to annual
41 precipitation uncertainty. This partial decoupling of streamflow generation from annual
42 precipitation makes forest restoration especially valuable for water supply during dry years or
43 in a drier future climate. Our study can increase confidence in the water resource benefits of
44 forest restoration in the central Sierra Nevada mountains, and our modeling framework is
45 widely applicable to forested mountain landscapes.

46 **1 Introduction**

47 Historical fire suppression (Stephens et al. 2016, van Wagtendonk et al. 2018) and
48 anthropogenic climate change (Seidl et al. 2017, Tague and Dugger 2010) have combined to
49 force North American conifer forests into an unstable ecosystem state (Marlon et al. 2012,
50 Schoennagel et al. 2017). As a result of fire exclusion policies, forests in the Sierra Nevada
51 mountains of California and Nevada are artificially homogenous and dense (Collins et al. 2011,
52 Dolanc et al. 2014, Taylor et al. 2014), which increases vulnerability to damaging megafires
53 (Skinner and Chang 1996, Steel et al. 2015, Goss et al. 2020, Safford et al. 2022) and negatively
54 impacts water security (Boisramé et al. 2017, Stephens et al. 2021b). Forest restoration,
55 including mechanical thinning and prescribed fire to restore historical disturbance frequencies
56 (North et al. 2007, Scholl and Taylor 2010, Kalies and Yocom Kent 2016, Stephens et al. 2021a),
57 can increase the resilience of forests (Hessburg et al. 2019, Knapp et al. 2021) and provide
58 societal benefits including reduced catastrophic fire risk (Loudermilk et al. 2016), stabilized
59 carbon storage (Liang et al. 2018, Cabiyo et al. 2021), wood products (Swezy et al. 2021, Elias et
60 al. 2023), increased ecological diversity (Stephens et al. 2021b), and increased water yield (Guo
61 et al. 2023, Chung et al. 2024).

62 Multi-benefit forest restoration frameworks may help fund restoration projects by
63 bundling convergent societal goals and economic incentives to build partnerships (Stephens et
64 al. 2021, Quesnel Seipp et al. 2023). The Tahoe Central Sierra Initiative (TCSI) is one such
65 partnership, focusing on multi-benefit resilience-based forest management plans for the

66 Truckee, Yuba, Bear, and American River basins (Manley et al. 2023). As part of the TCSI, the
67 U.S. Forest Service is assessing the feasibility of environmental markets for ecosystem services
68 such as water supply, carbon storage, and wood products. Several environmental markets could
69 potentially benefit from forest management tactics leading to more frequent tree removals and
70 controlled fire, aligned with partial or full restoration of the pre-colonial disturbance return
71 interval (van Wagendonk et al. 2018, Maxwell et al. 2022). In this study, we investigate the
72 potential impact of landscape-scale forest restoration scenarios developed by Maxwell et al.
73 (2022) on water resources in the TCSI region.

74 The possibility of increased water yield has incentivized forest thinning efforts for
75 decades, but the magnitude and even direction of post-disturbance streamflow changes varies
76 widely across western North America (Goeking and Tarboton 2022). It is broadly observed that
77 streamflow may increase if forest cover is reduced because of decreased evapotranspiration
78 (ET; Hibbert 1967, Bosch and Hewlett 1982, Troendle and King 1985). At the landscape scale,
79 however, the hydrological response to vegetation disturbance is more nuanced (Andréassian
80 2004), and ET can increase with a thinner canopy (Goeking and Tarboton 2020) due to a
81 combination of reduced shading (Morecroft et al. 1998), wetter soils (Boisramé et al. 2018), and
82 vegetation regrowth (Perry and Jones 2016). In their analysis of forest disturbance for 159
83 watersheds in the western U.S., Goeking and Tarboton (2022) found that energy-limited
84 watersheds are more likely to experience increases in streamflow associated with reductions to
85 forest cover compared to wetter and cooler watersheds. This mediating effect of aridity on
86 reductions in ET after vegetation disturbance is similarly observed locally in the Sierra Nevada
87 mountains, where more northerly (wetter) watersheds experience larger streamflow gains
88 following disturbance (Saksa et al. 2017). Previous studies in the TCSI region, which is part of
89 the wetter northern Sierra Nevada zone, have predicted substantial increases in streamflow
90 after wildfire or forest restoration (Saksa et al. 2020, Roche et al. 2018 and 2020, Guo et al.
91 2023). However, prior attempts to quantify landscape-scale streamflow changes usually rely on
92 extrapolation from a few years of pre- and post-disturbance measurements at the plot or small
93 catchment scale (e.g. Saksa et al. 2020, Roche et al. 2018). Landscape-scale forest restoration is
94 not an instantaneous nor homogenous process, and the hydrological effects of proposed multi-
95 decadal forest treatment plans (Maxwell et al. 2022) are further complicated by the role of
96 climate change in mediating ecohydrology in the coming decades (Tague and Dugger 2010).

97 Seasonal snowmelt controls water resources in much of western North America (Bales
98 et al. 2006), and there have been long-standing efforts to understand how forest management
99 might enhance the snowpack (Troendle 1983, Kattelman et al. 1983). A majority of studies
100 analyzed by Varhola et al. (2010) and Goeking and Tarboton (2020) associate thinner forests
101 with increased snow water equivalent (SWE). However, forest-snowpack relationships exhibit
102 considerable variability due to complex mass and energy interactions that are mediated by
103 climate and topographic controls. Reduced canopy interception tends to increase SWE,
104 particularly in areas with snowfall events near or below the canopy storage capacity (Storck et
105 al. 2002, Boon 2012, Winkler et al. 2012). However, increased shortwave radiation reaching the
106 snowpack in thinner forests can accelerate ablation, particularly in warmer climates and on
107 southern aspects, which results in reduced SWE after disturbance (Ellis et al. 2011, Harpold et

108 al. 2014, Tennant et al. 2017). Darker snow albedo in post-fire forests can compound the effect
109 of reduced shading, further accelerating snow ablation (Gleason et al. 2013). Due to the
110 competing interaction of interception and shading effects, as well as additional factors
111 including wind and thermal radiation from trees, many studies conclude that the snowpack
112 response to disturbance is a complex function of the local conditions and fine-scale forest
113 structure (e.g., Troendle 1983, Stevens 2017, Sun et al. 2018, Harpold et al. 2020). In the TCSI
114 region considered in this study, high resolution lidar and modeling studies indicate that snow
115 accumulation and meltwater inputs increase or decrease in different areas depending on the
116 interaction of canopy structure with solar radiation and wind (Lewis et al. 2023), and opening
117 gaps in dense canopies will promote snow accumulation and reduce ablation (Piske et al., in
118 press).

119 The effect of forest disturbance on net ET, and hence water yield, depends on a cascade
120 of complex factors (Moore and Heilman 2011, Adams et al. 2012). The different vapor loss
121 components of ET (i.e., transpiration and evaporation or sublimation from interception storage)
122 can be categorized depending on whether they are expected to increase or decrease in a
123 thinner forest (c.f. Figure 1 of Goeking and Tarboton 2020). Declines in transpiration have been
124 observed following tree mortality (Bales et al. 2018), which can reduce the soil moisture deficit
125 and thus support additional streamflow generation from future precipitation (Troendle 1979,
126 He et al. 2013, Boisramé et al. 2018). However, increased soil water availability sometimes
127 supports higher transpiration rates from the remaining trees that would otherwise be water-
128 limited, thereby capping streamflow gains during dry periods (Boisramé et al. 2019). Moreover,
129 aerodynamic effects and reduced shading can create a more arid microclimate and contribute
130 to increases in ET from remaining vegetation (Morecroft et al. 1998, Rambo and North 2009,
131 Ma et al. 2010, Meili et al. 2024), further limiting the streamflow response to disturbance
132 (Biederman et al. 2014, Meili et al. 2024). As a result, watershed-scale vapor loss can increase,
133 decrease, or remain relatively unchanged following severe forest disturbance (Goeking and
134 Tarboton 2020). Predicting the landscape-scale response to proposed management plans
135 requires modeling the interaction of topography, soils, snow, and vegetation over decades of
136 planned forest treatments under a changing climate.

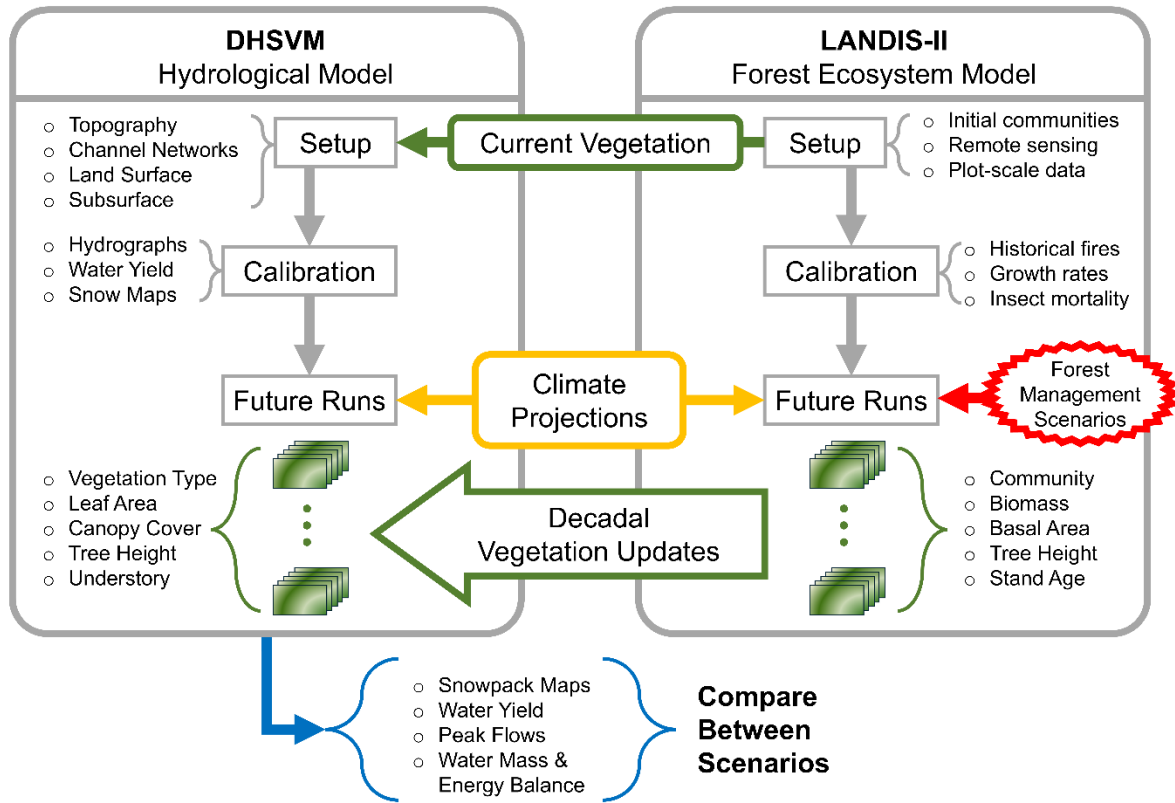
137 Forest disturbance generally increases peak streamflow (Goeking and Tarboton 2020),
138 but this response is dependent on the interaction of many processes. At small watershed
139 scales, peak flows tend to increase after disturbance due to interactions between elevated
140 antecedent water tables, reduced interception, increased snow accumulation, and faster
141 snowmelt (Lewis et al. 2001, Moore and Wondzell 2005, Pomeroy et al. 2012). Additionally,
142 natural or prescribed fires may contribute to peak flows through increased surface runoff from
143 hydrophobic soils (Certini 2005). The ancillary effects of mechanical thinning such as soil
144 compaction (Startsev and McNabb 2000) or the cutting of new forest roads can similarly alter
145 flow paths and increase peak flows (King and Tennyson 1984, Bowling and Lettenmaier 2002).
146 Peak flow increases on the order of 50% or more have been observed after forest disturbance
147 in catchments up to a few square kilometers in area (Moore and Wondzell 2005), but peak flow
148 impacts in larger-scale basins remain uncertain. Jones and Grant (1996) use the variable timing
149 of forest harvest to propose a statistical argument that forest disturbance may contribute to

150 substantially higher peak flows in watersheds as large as 600 km² in the Oregon Cascade Range,
151 though this finding is contradicted by reanalysis of the same data by Thomas and Megahan
152 (1998). Sierra Nevada watersheds face increased flood risks from anthropogenic climate change
153 (Huang and Swain 2022). Consequentially, the possible effects of forest restoration on peak
154 flows in the central Sierra Nevada requires consideration.

155 In this study, we address two of the unsolved problems in hydrology, namely the impact
156 of land cover change on water fluxes and the spatial variability in hydrologic extremes in
157 response to this change (Blöschl et al. 2019) by incorporating the outputs of a forest ecosystem
158 model into a distributed hydrological model to simulate the spatially explicit hydrological
159 effects of landscape-scale forest management scenarios. Forest management scenarios
160 considered here are based on input from the broader TCSI partnership (Maxwell et al. 2022), so
161 our hydrological investigation is uniquely grounded in detailed and plausible management
162 alternatives in a landscape-scale forest planning exercise. Using a novel combination of two
163 state-of-the-art models and a new Bayesian calibration method, we seek to answer the
164 following questions: (1) How much additional water yield would result from partial or full
165 restoration of the historic forest disturbance return interval in the central Sierra Nevada, and
166 which factors control variability in the sub-watershed response? (2) Could forest restoration
167 increase peak flows in ways that might accentuate flood risks to small- or large-scale
168 infrastructure? (3) How do the sources of uncertainty inherent in multi-decadal simulations
169 (climate, model uncertainty, and other unknowns) affect water resource planning?

170 **2 Methods**

171 Figure 1 outlines the three main components of this study. First, we set up and calibrate
172 a hydrological model using multiple types of historical water data. Second, we set up and
173 calibrate a forest ecosystem model to simulate vegetation responses to different forest
174 management scenarios. Third, we run the hydrological model to the end of the century using
175 climate projections and vegetation states from the forest ecosystem model. The following
176 sections address each of these components in detail.



177

178 **Figure 1.** Methodological flowchart for simulation procedures used in this study. Vegetation
 179 states simulated by the LANDIS-II forest ecosystem model are used to update the DHSVM
 180 hydrological model under different forest management scenarios.

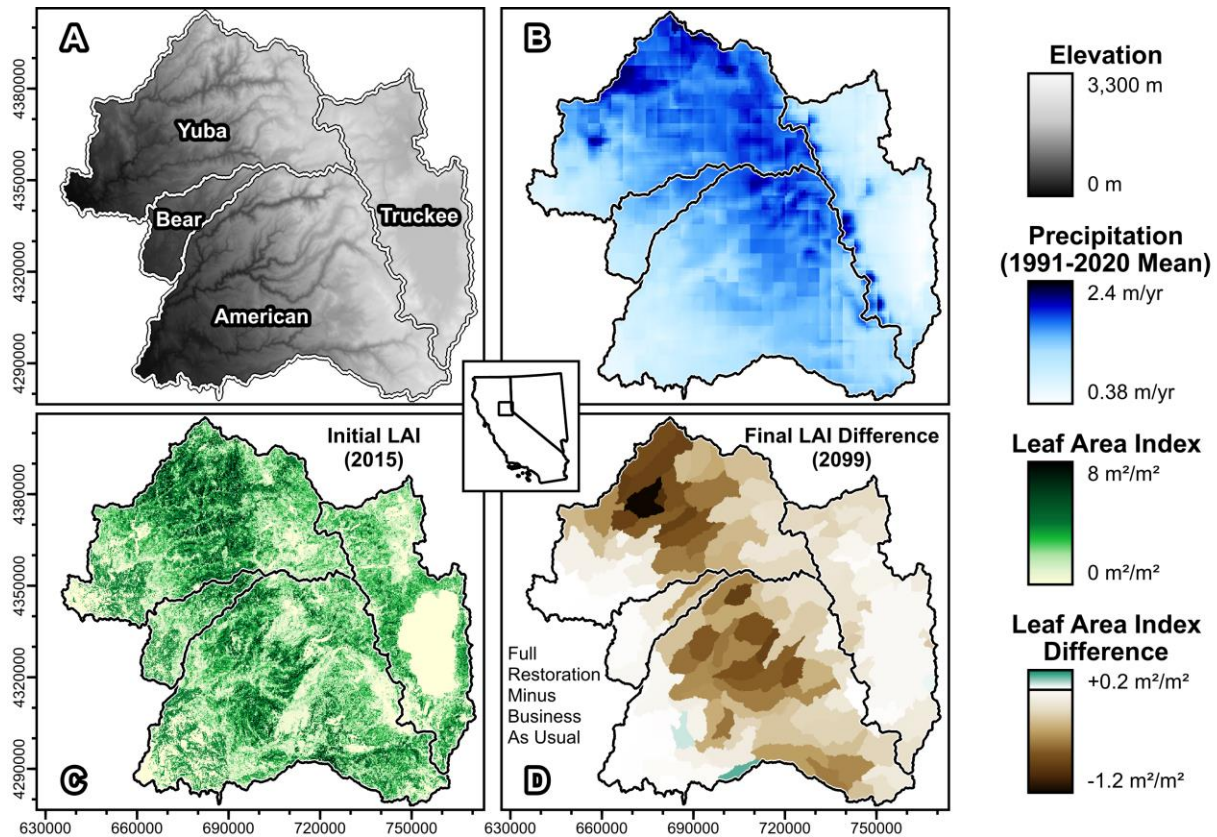
181 **2.1 Hydrological Modeling**

182 A physics-based, distributed-parameter approach to hydrological modeling enables us
 183 to quantify the interacting effects of forest restoration on hydrological processes and evaluate
 184 spatial heterogeneity in the watershed response to forest management scenarios. The
 185 Distributed Hydrology Soil Vegetation Model (DHSVM) was developed by Wigmosta et al.
 186 (1994, 2002) to simulate mountain watersheds with a particularly robust treatment of forest
 187 ecohydrological processes, such as overstory and understory interception and transpiration.
 188 DHSVM solves a water mass and energy balance on a two-dimensional grid, typically at high
 189 spatial resolution (90 m in this study) on a sub-daily timestep (3 hours in this study). The model
 190 represents vegetation with a two-layer “big leaf” approach that enables the separate
 191 calculation of overstory and/or understory interception storage, interception loss, and
 192 transpiration from three root zone soil layers in each grid cell. Streamflow in DHSVM is
 193 primarily generated from saturated subsurface discharge to a spatially explicit channel network,
 194 though overland flow paths are also included. Soil moisture is recharged by surface infiltration,
 195 and water in the saturated zone moves laterally through a shallow aquifer based on two-
 196 dimensional hydraulic gradients, approximated in this study from the local surface topography
 197 and spatially variable soil hydraulic conductivity. Compared to other process-based

198 ecohydrology models, DHSVM is notable for the high grid-scale resolution of its water mass and
199 energy balance and the high fidelity of its ecohydrological processes, which makes it particularly
200 suitable for simulating the hydrological effects of heterogeneous forest disturbances (see 30-
201 model intercomparison of Beckers et al. 2009).

202 2.1.1 Hydrological Model Setup

203 We combine literature review and a variety of spatial datasets to set up DHSVM for the
204 study region in the central Sierra Nevada mountains. The TCSI area includes four adjoining
205 watersheds, as shown in Figure 2: the Truckee River (2,273 km², mean elevation 2,100 m), the
206 Yuba River (3,435 km², mean elevation 1,305 m), the Bear River (585 km², mean elevation 821
207 m), and the American River (4,812 km², mean elevation 1,350 m). Topography is represented
208 using elevations from the Shuttle Radar Topography Mission (SRTM; Farr et al. 2007). Stream
209 networks are initiated with a minimum catchment area of 0.1 km², which is consistent with
210 imagery and the National Hydrography Database (NHD) channel network (U.S. Geological
211 Survey 2019). Textural soil data required for DHSVM are derived from POLARIS (Chaney et al.
212 2019), a high-resolution probabilistic remapping of the Soil Survey Geographic (SSURGO)
213 Database (Soil Survey Staff 2018). The multi-layer POLARIS data are vertically aggregated to
214 three root-zone depth layers up to 1.2 m depth (Jackson et al. 1996), plus a deep layer. The
215 Supporting Information includes an exhaustive description of inputs to DHSVM and their
216 estimation for this study, and relevant code is available online (see Availability Statement).



217

218 **Figure 2.** Maps of the Tahoe-Central Sierra project area: (A) digital elevation model; (B) mean
 219 yearly precipitation; (C) pre-restoration leaf area index (LAI); (D) final LAI difference between
 220 the full-restoration (S6) and business-as-usual (S2) management scenarios aggregated by sub-
 221 watershed. Inset map shows the study area location in the U.S. states of California and Nevada.

222 The parameterization of vegetation in DHSVM requires particular attention to robustly
 223 estimate the effects of forest restoration. Spatially explicit maps of vegetation type, canopy
 224 fractional cover, overstory monthly leaf area index (LAI), tree height, and dense understory
 225 presence are derived from outputs of the forest ecosystem model (Section 2.2). Where dense
 226 understory is not indicated, we assume a light understory presence beneath the forest canopy
 227 based on field experience in the study region, which indicates a typical lack of bare soil.
 228 Understory is parameterized with a constant LAI of $3 \text{ m}^2/\text{m}^2$ for dense understory or $1 \text{ m}^2/\text{m}^2$
 229 for light understory based on field estimates of LAI for shrub ecosystems common to the study
 230 area (Hughes et al. 1987 and McMichael et al. 2004). Through manual sensitivity tests, we find
 231 that most vegetation parameters are insensitive to minor perturbations in the study region, so
 232 these parameters are maintained at baseline values used elsewhere in the DHSVM literature.
 233 One particularly sensitive parameter is the minimum stomatal resistance, which controls
 234 overstory transpiration for each vegetation type. We conduct a review of 18 species-level
 235 stomatal conductance field studies to estimate minimum resistance values and uncertainties
 236 for 15 distinct DHSVM vegetation types with at least two literature estimates per type (see
 237 Supporting Information). Canopy interception parameters are estimated from numerous field
 238 studies using the literature review summaries compiled by Link et al. (2004) for rain and Martin

239 et al. (2013) for snow. Finally, abiotic land surfaces including water, urban, and rock types are
240 mapped using the National Land Cover Database (NLCD; Dewitz and U.S. Geological Survey
241 2019) and represented in DHSVM with impermeable areas and detention storage (Cuo et al.
242 2008).

243 Meteorological forcing data for DHSVM are generated using a variety of spatiotemporal
244 disaggregation techniques. Historic meteorological data are obtained from gridMET
245 (Abatzoglou 2013), and future climate projections are obtained from the analogous
246 Multivariate Adaptive Constructed Analogs (MACA) downscaled global circulation model (GCM)
247 dataset (Abatzoglou and Brown 2012). Both climate datasets provide daily precipitation,
248 minimum/maximum temperature, and wind speed at 4 km resolution. The model requires
249 inputs of precipitation, air temperature, relative humidity, wind speed, incoming shortwave
250 radiation, and incoming longwave radiation. We temporally disaggregate the daily data to the
251 3-hour DHSVM timestep and simulate the additional required variables using MetSim (Bennett
252 et al. 2020), which is based on the MTCLIM model (Hungerford et al. 1989). Precipitation is
253 assumed constant within each day, which is a reasonable assumption for the multi-day cold-
254 season storms typical of the central Sierra Nevada (e.g. Huning and Margulis 2017), but we
255 acknowledge that this assumption could affect assessments of rain-driven peak flow events. We
256 spatially disaggregate 4 km gridMET precipitation data using monthly redistribution maps
257 calculated from 800 m PRISM normals (PRISM Climate Group 2022) to exactly preserve the
258 spatial mass balance of the 4 km data while redistributing precipitation approximately
259 proportional to the monthly PRISM normals within each 4 km cell (Figure 2B). Preserving the
260 exact gridMET precipitation mass balance is a priority in this study for the sake of consistency
261 with the gridMET forcing data used for LANDIS-II, so we eschew common downscaling
262 techniques that are not mass-preserving, such as bilinear interpolation. Temperature data are
263 spatially disaggregated to the 90 m DHSVM grid scale using spatially variable monthly lapse
264 rates calculated by linear regression of elevation versus PRISM monthly temperature normals
265 for the 25 800 m cells within each 4 km gridMET cell. In the study region, there are 193 gridMET
266 cells covering the Truckee watershed, 295 covering the Yuba watershed, 65 covering the Bear
267 watershed, and 385 covering the American watershed. Baseline DHSVM parameters controlling
268 snowpack accumulation and ablation are set based on the results of Sun et al. (2018) for the
269 Sierra Nevada region.

270 2.1.2 Hydrological Model Calibration

271 We refine our baseline setup of DHSVM with calibration of key parameters. Manual
272 sensitivity tests reveal seven parameters that are sensitive to perturbation within the a priori
273 uncertainty range of available data: mean soil depth [m], hydraulic conductivity [m/s], the
274 exponential decrease in hydraulic conductivity with depth [-], porosity [%], minimum stomatal
275 resistance [s/m], the maximum air temperature for snowfall [°C], and the melt-season albedo
276 decay rate [-]. Soil depth is calibrated using an offset applied to a baseline pattern based on
277 topographic curvature (Patton et al. 2018) to generate a mean soil depth between 1.3 and 4 m
278 based on the minimum required to satisfy the rooting depth and upper-bound sensitivity tests.
279 Hydraulic conductivity and porosity are calibrated between the 5th, 50th, and 95th percentile

280 values for each grid cell and soil layer provided by the POLARIS data (Chaney et al. 2019).
281 Single-valued parameters are calibrated over a prior range determined from variability
282 observed in the literature or manual sensitivity tests, as outlined in the Supporting Information.
283 All parameters and maps are maintained within plausible physical ranges, and all four major
284 TCSI basins are calibrated together to improve generality.

285 To quantify uncertainty in key hydrological processes, we evaluate six objective functions
286 targeting different hydrological signatures. The selected objective functions are daily
287 streamflow Nash-Sutcliffe Efficiency (NSE), log-scale NSE for two sets of sub-watersheds
288 exhibiting comparatively high or low baseflows, root mean squared error (RMSE) for yearly
289 water yield at large scales, RMSE for 95th-percentile high flows at large scales, and pixel-wise
290 RMSE for yearly peak SWE. The calibration period is defined as water years 2012-2017 for
291 streamflow data (not counting one year of model spin-up) in order to capture a range of
292 variability, including a multi-year drought (2013-2015) and one of the wettest years in recent
293 decades (2017). Unimpaired or reconstructed daily streamflow timeseries are obtained for 10
294 stream gauges in the Truckee and Yuba watersheds (U.S. Geological Survey 2022; refer to
295 calibration figures in Supporting Information for gauge numbers). Large-scale flows are
296 constrained with reconstructions of natural streamflow at the YRS flow point (California
297 Department of Water Resources 2022). Yearly pixel-wise peak SWE maps are calculated for the
298 Yuba and Truckee watersheds from the Margulis et al. (2016) snow reanalysis for water years
299 2011-2016.

300 We apply multi-objective Bayesian optimization to the sensitive parameters identified
301 previously in order to minimize errors in each objective function and quantify residual
302 hydrological uncertainty. In Bayesian optimization, objective functions are modeled using
303 stochastic processes as surrogates for the underlying model (DHSVM in our case), which boosts
304 calibration efficiency (Jones et al. 1998). Starting with an initial minimax Latin hypercube
305 sample of the seven-dimensional parameter space (Morris and Mitchell 1995, implemented by
306 Dupuy et al. 2015), we use Gaussian Process regression (Rasmussen and Williams 2008,
307 implemented by Roustant et al. 2012) to build surrogate models of each objective, and optimize
308 the expected hypervolume improvement of subsequent parameter sets (Emmerich et al. 2011,
309 implemented by Binois and Picheny 2019) with parallel particle swarm optimization (Kennedy
310 and Eberhart 1995, implemented by Zambrano-Bigiarini et al. 2013). After testing a total of 300
311 unique parameter sets during 6 rounds of optimization, we identify Pareto-efficient designs,
312 which constitute the set of models where improving one objective requires worsening another.
313 From this Pareto set of calibrated models, we select three high-performing models that are
314 representative of the tradeoffs between objective functions and the residual uncertainty in
315 calibration parameters (SI Figures S1-S3). We validate the selected models over water years
316 2006-2011. During validation, we expand our objective functions to include two additional
317 stream gages and reconstructed natural flows in the American River watershed at the AMF/NAT
318 flow point below Folsom Lake (California Department of Water Resources 2022).

319 2.1.3 Hydrological Model Future Runs

320 We simulate the long-term hydrological effects of forest restoration by running DHSVM
321 subject to future climate projections and updating vegetation maps to reflect spatiotemporal
322 heterogeneity associated with forest disturbances, management, and regrowth. We select the
323 CNRM-CM5 (Voldoire et al. 2013) and MIROC5 (Watanabe et al. 2010) climate projections since
324 these models represent endmembers for fire weather in the central Sierra Nevada study region
325 (Maxwell et al. 2022), with CNRM-CM5 representing a relatively wet scenario, and MIROC5
326 representing a relatively dry scenario. We select the RCP-8.5 pathway for both GCMs since this
327 higher-emissions scenario fits likely behaviors in the near to mid-future (Schwalm et al. 2020).
328 On average within the project area, the CNRM-CM5 climate projection has a temperature trend
329 (Sen 1968) of 0.062 °C/yr, amounting to a 5.3 °C increase over the 85-year simulation period,
330 with mean precipitation of 597 mm/yr. The MIROC5 climate has a temperature trend of 0.045
331 °C/yr, amounting to a 3.9 °C increase over 85 years, with 456 mm/yr mean precipitation (24%
332 less than CNRM-CM5). GCM projections are further disaggregated and downscaled from the
333 Abatzoglou and Brown (2012) MACA dataset using the same methodology outlined above for
334 consistency with the forcing data on the historic calibration and validation periods.

335 The effect of ongoing forest restoration is represented in DHSVM with updated maps of
336 vegetation type, canopy fractional cover, overstory LAI, tree height, and dense understory
337 presence every ten years. Updated vegetation maps are ingested into DHSVM on October 1st
338 five years prior to the date that they represent. Offsetting the dates with this approach enables
339 DHSVM to simulate hydrological conditions for each set of vegetation maps over a 10-year
340 period centered on the year corresponding to the updated vegetation maps. More frequent
341 (e.g., yearly) updates of the DHSVM vegetation maps could better resolve rapid changes near
342 the beginning of the treatment period, but we find that decadal updates can satisfactorily
343 resolve relatively slow trends in the forest landscape after the first decade of treatment.

344 2.2 Forest Ecosystem Modeling

345 To model change in vegetation over time and in response to climate and management,
346 we used the LANDIS-II forest landscape model (Scheller et al. 2007) with parameterization
347 following Maxwell et al. (2022). LANDIS-II is a flexible modeling framework that allows for
348 varying extensions to model vegetation dynamics and disturbance in a spatially explicit gridded
349 format allowing communication among cells (e.g, by seed dispersal or fire spread). In this study,
350 we also use the Net Ecosystem Carbon and Nitrogen (NECN v6.9) succession extension (Scheller
351 et al. 2011). NECN is a mechanistic succession model which tracks cohorts of trees (each with
352 associated age, species, and biomass) as they grow, reproduce, recruit, and senesce. Cohort
353 growth and establishment depend on site conditions (e.g., climate, soils) and competition with
354 other cohorts for water, growing space, and soil nitrogen. NECN tracks carbon and nitrogen
355 through multiple biomass and soil compartments. In NECN, climate has emergent effects on
356 ecosystem processes through its impact on vegetation growth, respiration, and soil carbon
357 dynamics. All model parameters and installers needed to reproduce our TCSI forest ecosystem
358 model are available online (see Open Research section).

359 2.2.1 Forest Ecosystem Model Setup and Calibration

360 The initial (year 0) landscape of the LANDIS-II model is derived from multiple data
361 sources. Initial vegetation conditions are generated from Forest Inventory and Analysis (FIA)
362 plots (Burrill et al. 2021) imputed from Landsat remote sensing products with soil data from
363 SSURGO. We model several key disturbance processes, including fire (natural ignition and
364 prescribed), insect pests, and harvest (through implementation of the management scenarios).

365 To model wildfire and prescribed fire, we use the Social-Climate-Related Pyrogenic
366 Processes and their Landscape Effects (SCRPPLE v3.2.3) extension (Scheller et al. 2019), a data-
367 driven empirical model of fire spread, fire intensity, and tree mortality. SCRPPLE simulates fire
368 spread, intensity, and mortality depending on fuels, weather, and topography. The fire
369 parameters are calibrated to ignitions data (Short 2021), daily fire perimeters from the National
370 Interagency Fire Center (NIFC 2019) and fire severity maps from Monitoring Trends in Burn
371 Severity (Eidenshink et al. 2007). Tree mortality is parameterized using the Fire and Tree
372 Mortality Database (Cansler et al. 2020). For details, refer to the appendix of Maxwell et al.
373 (2022).

374 Insect pests are simulated using the Biomass Biological Disturbance Agents (Biomass-
375 BDA) extension, modified from BDA v2.1 (Sturtevant et al. 2004), which simulates outbreaks of
376 pests and pathogens as a spatially contagious process dependent upon climate and host
377 availability. We simulate fir engraver (*Scolytus ventralis*), Jeffrey pine beetle (*Dendroctonus*
378 *jeffreyi*), mountain pine beetle (*D. ponderosae*), and western pine beetle (*D. brevicomis*), as
379 well as white pine blister rust (*Cronartium ribicola*). We calibrate outbreak patterns using USFS
380 Aerial Detection Survey and Ecosystem Disturbance and Recovery Tracker data (Koltunov et al.
381 2020). The extent and severity of outbreaks is an outcome of climate, host tree density, and
382 spatial patterning, allowing for complex interactions among climate, vegetation, management,
383 and hydrology (Scheller et al. 2018).

384 2.2.2 Forest Management Scenarios

385 We utilize several previously developed scenarios (Maxwell et al. 2022) to represent a
386 range of management activities ranging from very little management to approximately full
387 restoration of a natural disturbance return interval. The scenarios' overall objectives are to
388 restore forest ecosystems to a state that is more similar to their character prior to fire
389 exclusion. The scenarios attempt to restore a low- or mixed-severity fire regime by
390 reintroducing disturbances in the form of prescribed fire or thinning from below. The
391 proportion of the landscape treated per year depends upon the historical fire-return interval of
392 the management zone, but ranges from ~1% to ~6% per year across the whole landscape. We
393 implement harvests using the Biomass-Rank Biomass Harvest extension, a modification of
394 Biomass Harvest that allows greater flexibility in selecting locations to harvest based on their
395 biomass. Management zones are developed using land ownership and land use, slope
396 steepness, and historical fire return interval data from LANDFIRE (U.S. Department of the
397 Interior 2016). Within all scenarios, private lands are managed as business-as-usual, with pre-
398 commercial thinning and clearcuts on private timberlands. The wildland-urban interface (WUI)

399 Defense zone (within 400 m of settlements) is also treated for fuel reduction in all scenarios.
400 The scenarios are described in detail by Maxwell et al. (2022) and summarized here. Note that
401 the scenario names given here are selected for interpretability with reference to our
402 hydrological results, and the concept of “business-as-usual” is not prescriptive but rather
403 reflects a baseline level of management in the simulations.

404 *1. Reduced treatment.* Management is restricted to fuel treatments within the WUI Defense
405 zone (within 400 m of settlements) and private lands. This scenario represents a substantial
406 reduction in general forest treatment compared to present-day management.

407 *2. Business-as-usual (BAU).* This scenario is designed to closely match management practices in
408 the present and recent past, including private land management and management of general
409 forests as recorded in USFS and CalFire databases.

410 *3. Partial restoration with less fire.* In this scenario, treatments are extended to general forest
411 and roadless areas. Almost all treatments are either mechanical thinning or hand thinning,
412 depending upon the slope steepness and land use category. Prescribed fire is used for 5% of
413 treatments on general forest land and 20% of treatments in roadless areas.

414 *4. Partial restoration.* This scenario is similar to Scenario 3, but it replaces 20% of the thinning
415 treatments in the WUI Threat zone with prescribed fire.

416 *5. Full restoration with less fire.* This scenario and Scenario 6 attempt to replicate the historical
417 disturbance return interval (~6% of the landscape treated per year). The types of treatment and
418 kinds of stands treated are identical to Scenario 4, but the area treated per year is greater.

419 *6. Full restoration.* Compared to Scenario 5, this scenario increases the amount of prescribed
420 fire: 30% of treatments in general forest and roadless areas use fire rather than mechanical
421 thinning treatments.

422 2.2.3 Forest Ecosystem and Hydrological Model Linkage

423 In order to assess the emergent effects of forest management and disturbance on water
424 resources, we translate outputs from LANDIS-II into suitable inputs for DHSVM. LANDIS-II
425 generates several outputs natively which can be directly used in DHSVM, including LAI (Figure
426 2C) and species composition (SI Figure S14), but other outputs require further processing. To
427 create inputs for fractional canopy cover, we use regression models from FIA data. For details,
428 refer to the appendix of Zeller et al. (2023). Because the LANDIS-II model is parameterized from
429 forest inventory data, understory vegetation is underrepresented in the vegetation layers,
430 which could bias the hydrological model. To impute understory vegetation cover, we use FIA
431 data to create beta regression models predicting understory shrub cover as a function of tree
432 biomass, tree age, canopy cover, and forest type. We classify sites as having dense understory if
433 the regression model predicts understory shrub cover exceeding 20%. Sites without a shrub
434 understory have an assumed light understory cover in DHSVM, typical of grasses and forbs in
435 the study area, as discussed in the hydrological modeling section.

436 2.3 Output Processing and Scenario Comparisons

437 Comparing simulated watershed behaviors between different restoration scenarios
438 enables us to attribute variable hydrological dynamics to forest management actions.
439 Differences in modeled maps of yearly pixel-wise peak SWE and snowmelt timeseries can
440 quantify forest disturbance impacts on snowpack dynamics. We use simulated streamflow
441 timeseries to estimate additional reservoir inflow volumes attributable to forest restoration,
442 and we construct flow duration curves (Vogel and Fennessey 1995) to assess impacts on the
443 high flow regime. Finally, aggregated timeseries of water mass balance fluxes enable us to
444 calculate differences in the partitioning of landscape-average yearly overstory and understory
445 transpiration, overstory and understory interception loss, and streamflow generation.

446 We analyze the effects of forest restoration on local streamflow generation and peak
447 flows using sub-watershed daily streamflow timeseries. During each DHSVM run, we save
448 streamflow records at 139 selected pour points approximately corresponding to the HUC-12
449 watersheds represented in the NHD watershed boundary dataset (U.S. Geological Survey 2019).
450 We calculate yearly local streamflow generation for each sub-watershed by subtracting
451 streamflow contributions from any upstream tributaries. Comparing streamflow generation in
452 different management scenarios isolates the effect of forest restoration. To analyze peak flow
453 effects, we compute the Sen's slope (Sen 1968) for one-day yearly peak flows in each sub-
454 watershed across the full 85-year period. By differencing the peak flow trends for each sub-
455 watershed under different management scenarios, we ascertain the effect of forest restoration
456 on one-day yearly peak flows. This approach isolates the effects of each management scenario
457 by removing climate-induced peak flow trends from the business-as-usual scenario.

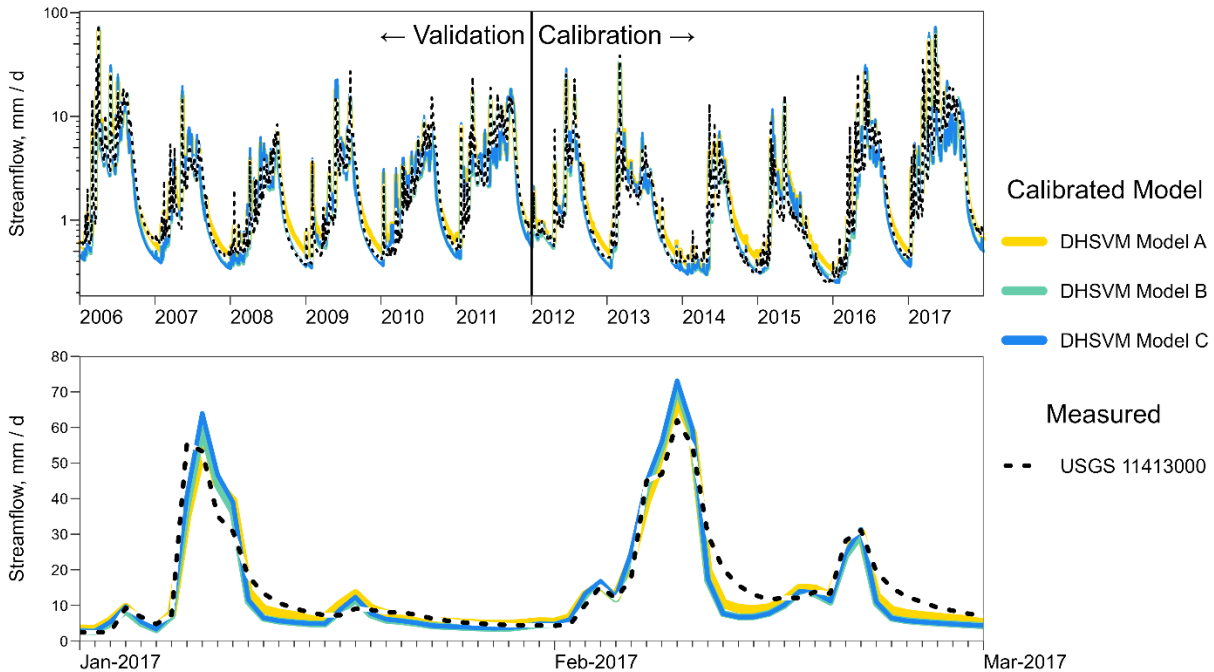
458 To investigate peak flow connections to forest restoration, we isolate major storm
459 runoff events and compare contemporaneous water balance fluxes between different
460 management scenarios. Since we model the study region with four separate watershed
461 domains, three DHSVM models, and two GCMs, we obtain a total of 24 watershed-aggregated
462 timeseries. In each timeseries, we identify yearly peak flow dates across the 85-year simulation
463 period. For peak flow events preceded by multiple days of continuous precipitation, we define a
464 storm period extending from the first day with more than 1 mm/d of precipitation through the
465 day of the yearly peak flow. For each such event, we calculate precipitation intensity as the
466 mean daily precipitation rate during the storm period. For the 10 highest-intensity precipitation
467 events prior to yearly peak flows in each combination of watershed, DHSVM model, and GCM,
468 we calculate storm-total interception by subtracting the total overstory and understory
469 interception storage (rain plus snow) on the first day of the continuous storm period from the
470 total interception storage on the peak flow date. We similarly calculate cumulative interception
471 vapor loss, snowpack outflow, and snow energy balance fluxes over the same storm periods.

472 **3 Results**

473 3.1 Hydrological Model Calibration and Validation

474 We select three Pareto-efficient DHSVM parameter sets from our multi-objective
475 Bayesian calibration based on tradeoffs between simulation accuracy for the snowpack,
476 baseflows, yearly water yield, and high flows. Model A achieves the highest area-weighted daily
477 NSE across all calibration watersheds, Model B has the lowest RMSE for large-scale high flows,
478 and Model C has the lowest yearly water yield RMSE subject to the requirements of daily NSE >
479 0.8 and high-flow daily RMSE < 80 m³/s. The three selected models are Pareto-efficient for all
480 six calibration objective functions and representative of the residual uncertainty in the
481 calibration parameter space. Model A is notable for having relatively low porosity and a slower
482 decrease in transmissivity with depth (deep layer average porosity of 0.40 compared to 0.53 in
483 Model B and 0.54 in Model C). Model B is notable for having relatively deep soil (3.8 m average
484 compared to 2.8 m in Model A and 2.4 m in Model C). Model C is notable for having relatively
485 low transpiration rates (average minimum stomatal resistance across conifer classes of 260 s/m
486 compared to 189 s/m in Model A and 187 s/m in Model B). All three selected models have
487 relatively high effective hydraulic conductivities, near the 95th percentile of the POLARIS data
488 (Chaney et al. 2019), with snow parameters converging reasonably close to those estimated by
489 Sun et al. (2018) for the Sierra Nevada region.

490 The ensemble of calibrated DHSVM models reproduces key hydrological signatures
491 during historic calibration and validation periods. During the calibration period (water years
492 2012-2017), the three selected models achieve a mean area-weighted daily NSE of 0.82 across
493 all 10 gauged watersheds, with an area-weighted NSE of 0.75 indicating a moderate decrease in
494 skill on the validation period (water years 2006-2011). The decrease in NSE during the
495 validation period could be caused in part by lower year-to-year variability in streamflow, which
496 reduces the total sum of squares (denominator of NSE). In the North Yuba watershed (USGS
497 station 11413000), which is the largest gauged basin without upstream flow regulation in our
498 study area (650 km²), the calibrated models produce a mean daily NSE of 0.87 over the
499 calibration period and 0.80 over the validation period (Figure 3). In log-transformed space, the
500 calibrated models produce calibration and validation NSEs of 0.94 and 0.92 in the North Yuba,
501 indicating that DHSVM is satisfactorily reproducing both low-flow and high-flow regimes at this
502 gauge, including major peak flows associated with rain-on-snow events in the winter of 2017
503 (Figure 3). Daily NSEs are more variable in smaller watersheds (11-130 km²), typically in the
504 range of 0.6 to 0.8 for both calibration and validation periods with occasional larger errors
505 associated with incorrect rain-snow partitioning at the ~10 km² scale in steep terrain (refer to
506 Supporting Information for a full set of hydrographs). At full watershed scales, DHSVM shows
507 low bias in water yield, with bulk runoff errors of -8% to +2% at the YRS and AMF full natural
508 flow points during calibration and validation periods (mean error -3% across all models and
509 periods at both measurement points). The calibrated models also satisfactorily reproduce
510 variability in large-scale peak flows, pixel-wise maximum yearly SWE, and pixel-wise maximum
511 yearly SWE timing (SI Figures S4-S13).



512

513 **Figure 3.** Example calibration and validation hydrographs for DHSVM. The North Yuba (USGS
 514 station 11413000) is the largest gauged watershed in the study area that has negligible
 515 upstream diversion or flow regulation. The model is calibrated on a total of 10 watersheds and
 516 validated on a total of 12 watersheds (refer to Supporting Information for additional calibration
 517 and validation hydrographs).

518 3.2 Forest Ecosystem Response to Disturbance

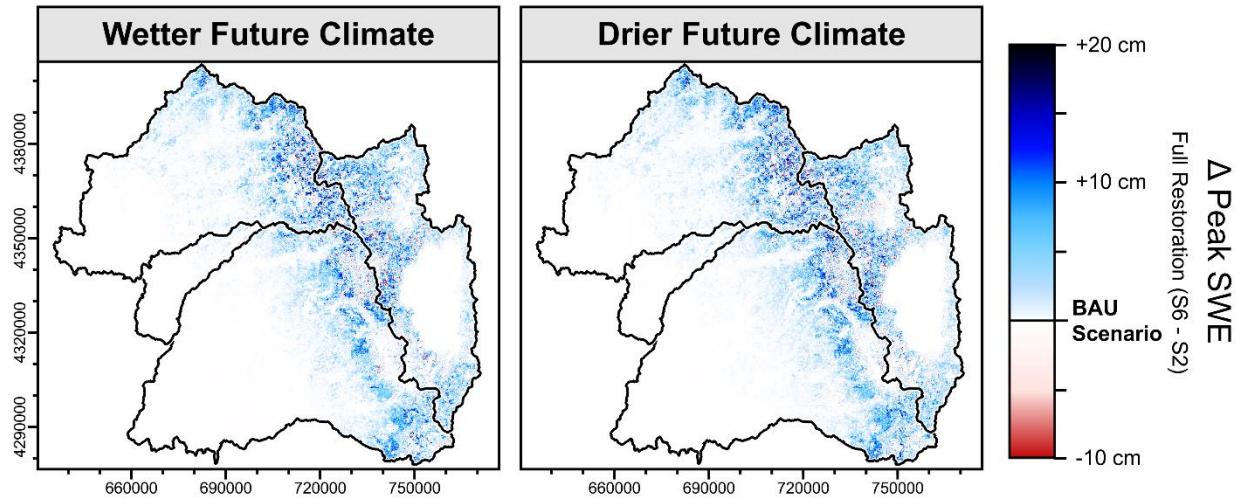
519 The LANDIS-II forest ecosystem model produces spatially explicit timeseries of
 520 vegetation characteristics across a spectrum of prescribed forest management scenarios.
 521 Conifer forests cover most of our central Sierra Nevada study region with the exception of high
 522 alpine regions and lakes, most notably Lake Tahoe. The historical baseline map from LANDIS-II,
 523 used for DHSVM calibration, has an area-averaged grid cell LAI of $2.3 \text{ m}^2/\text{m}^2$, with a median of
 524 $2.2 \text{ m}^2/\text{m}^2$ and a 90th percentile of $4.5 \text{ m}^2/\text{m}^2$. The densest forests are historically concentrated
 525 at mid-elevations on the west slope of the mountain range (Figure 2C).

526 Partial or full restoration of the historic forest disturbance return interval produces
 527 relatively thinner forests. Regardless of management scenario, LANDIS-II indicates a substantial
 528 decrease in forest density by the end of the century primarily from increased insect mortality
 529 (Maxwell et al. 2022). In the business-as-usual scenario (S2), LANDIS-II shows a mean LAI of 1.5
 530 m^2/m^2 at the end of the century (median $1.3 \text{ m}^2/\text{m}^2$ and 90th percentile $3.4 \text{ m}^2/\text{m}^2$), which is a
 531 decrease of 33% relative to the pre-restoration mean (averaged across both climates).
 532 Comparatively, the reduced treatment scenario (S1) shows a 32% decrease in mean LAI, the
 533 partial restoration scenarios show a 36% decrease in mean LAI (both S3 and S4), and the full
 534 restoration scenarios show a 43% (S5, less fire) or 47% (S6, more fire) decrease in mean LAI

535 over the same 85-year period. At the end of the century, mean LAI in the full restoration (S6) is
536 $0.31 \text{ m}^2/\text{m}^2$ lower (-14%) compared to the business-as-usual scenario (S2). Scenario differences
537 in post-restoration LAI are largest in the same mid-elevation west slope regions that have the
538 densest initial forest cover (Figure 2C-D), up to a maximum sub-watershed difference of 1.2
539 m^2/m^2 (39%) between full restoration and business-as-usual scenarios. In all scenarios and both
540 climates, LANDIS-II predicts significant species changes during the 85-year simulation period;
541 most notably, white fir (*A. concolor*) cover substantially decreases and Douglas fir (*P. menziesii*)
542 cover increases. Additionally, understory cover increases at higher elevations regardless of
543 management scenario. Refer to SI Figure S14 for maps of initial and final vegetation types and
544 understory LAI.

545 3.3 Simulated Effects on the Snowpack

546 In restoration scenarios with a relatively thinner forest canopy, DHSVM predicts
547 relatively higher landscape-average snowpack accumulation. A pixel-wise average of the peak
548 yearly SWE in all three models and all 85 years provides a spatial metric for snow accumulation
549 during the simulation period (Figure 4). Compared to business-as-usual (S2), the mean pixel-
550 wise peak SWE in the full restoration scenario (S6) is about 5% higher in the wetter CNRM-CM5
551 climate and about 6% higher in the drier MIROC5 climate. In both climates, the absolute
552 magnitude of peak SWE differences between S6 and S2 varies between about -5 and +12 cm
553 (1st and 99th percentiles). The spatial heterogeneity of SWE accumulation effects is only slightly
554 lower (-4 to +13 cm) when only considering grid cells where LAI is lower in S6 than S2 to
555 account for the effect of stochastic disturbance locations in LANDIS-II outputs. Thus, most of
556 the modeled heterogeneity in the snowpack response to forest thinning (Figure 4) is
557 attributable to meaningful differences in the model response to forest structure rather than
558 merely spatial noise resulting from the stochasticity of the prescribed treatments. We observe
559 that the percent change in pixel-wise peak SWE is relatively consistent throughout the
560 simulation period, but the effect begins to attenuate during the 2070s-2090s as precipitation
561 increasingly falls as rain in a warmer future climate (SI Figure S15). The pixel-wise snow ablation
562 rate, calculated from the peak SWE date to the melt-out date, also increases by around 1-10%
563 in most years, except late in the century when thinner forests melt out marginally slower (SI
564 Figure S16).



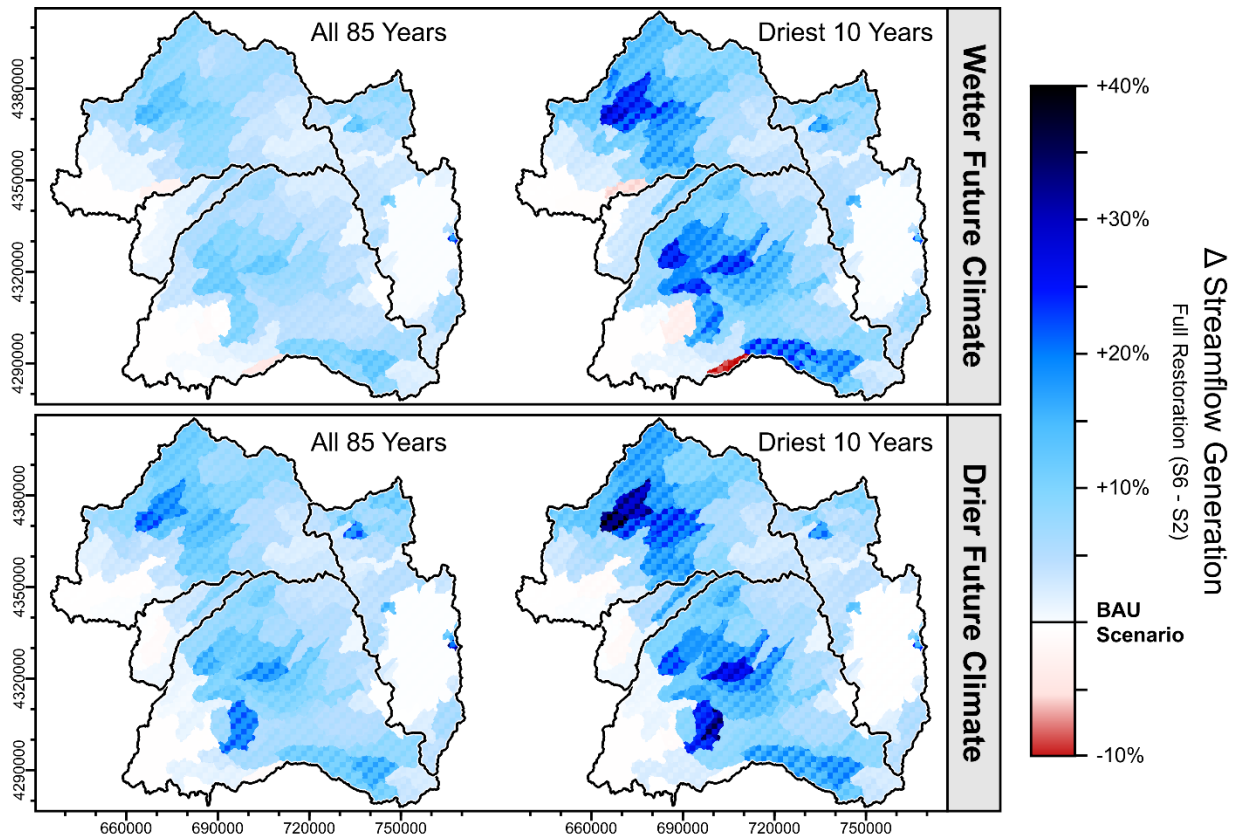
565

566 **Figure 4.** Difference in pixel-wise peak snow water equivalent (SWE) between the full
 567 restoration (S6) and business-as-usual (BAU, S2) forest management scenarios, calculated as an
 568 average over the full 85-year period under the CNRM-CM5 (wetter) and MIROC5 (drier) RCP 8.5
 569 climate projections.

570

3.4 Simulated Effects on Streamflow Generation

571 DHSVM predicts an increase in streamflow generation from forested sub-watersheds in
 572 the central Sierra Nevada with an increased pace of forest restoration (Figure 5). On average
 573 over the 85-year simulation period across the whole study area and all three models, DHSVM
 574 predicts 4.3% more total streamflow generation in S6 relative to S2 under the wetter CNRM-
 575 CM5 climate, and 5.7% more total streamflow generation under the drier MIROC5 climate.
 576 However, the effect of forest restoration on local streamflow generation is heterogeneous in
 577 space and time. In certain sub-watersheds, the average 85-year streamflow change is as high as
 578 +27% in the drier climate and +22% in the wetter climate. Conversely, the effect is near zero in
 579 sub-watersheds with low initial forest cover. Decreases in streamflow generation (as low as -
 580 4%) are observed where forest cover is locally denser in S6 than in S2, a result of stochasticity in
 581 the spatial distribution of fires between different LANDIS-II runs. Averaging over only the driest
 582 10 years in each climate projection, sub-watershed streamflow generation increases by up to
 583 +35% under the drier MIROC5 climate (median = +6%, 90th percentile = +18%) and up to +27%
 584 in the wetter CNRM-CM5 climate (median = +7%, 90th percentile = +18%). In summary,
 585 restoring a more frequent disturbance return interval to Sierra Nevada forests has the greatest
 586 relative effect on streamflow generation during dry years.



587

588 **Figure 5.** Percent difference in local streamflow generation for 139 sub-watersheds in the full-
 589 restoration (S6) forest management scenario relative to the business-as-usual (BAU, S2)
 590 scenario, calculated as an average over the full 85-year period and as an average over the driest
 591 10 years in each climate. The checkerboard pattern is produced by interweaving results from
 592 three calibrated DHSVM models, thus representing uncertainty in the hydrological model.

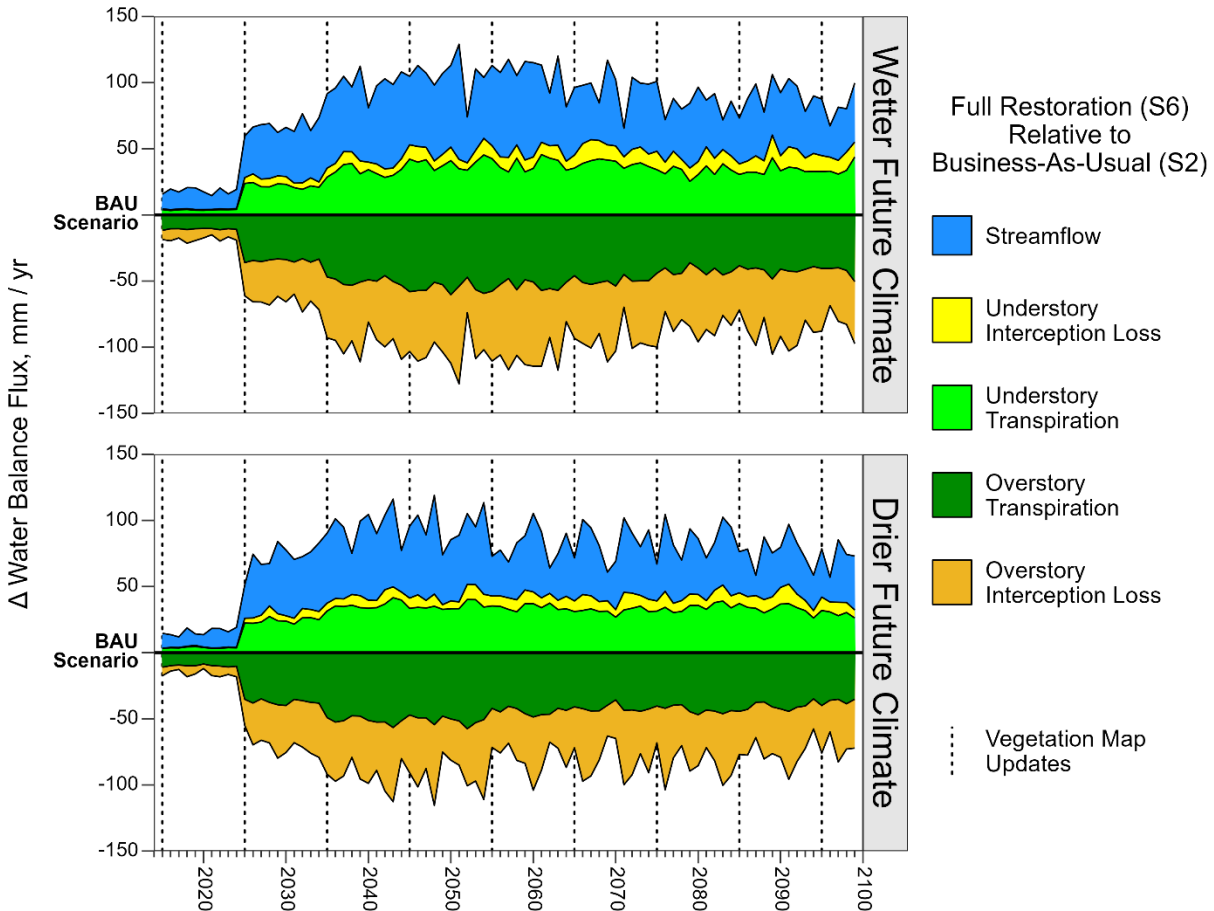
593 Sub-watersheds show significantly different streamflow generation responses
 594 depending on the local climate and initial forest conditions. The absolute streamflow
 595 generation response to forest restoration (S6 – S2) in units of water depth (SI Figure S17) has a
 596 median of 45 mm/yr or 39 mm/yr, a 90th percentile of 93 mm/yr or 82 mm/yr, and a maximum
 597 of 151 mm/yr or 142 mm/yr in the wetter (CNRM-CM5) and drier (MIROC5) climates,
 598 respectively. Spatial heterogeneity in the absolute (not percentage) effect on streamflow
 599 generation correlates with the sub-watershed mean historical LAI (Pearson correlation $r = 0.69$),
 600 the LAI difference between scenarios at the end of the century ($r = 0.93$), and precipitation ($r =$
 601 0.64), with no linear correlation to elevation ($r = 0.14$). Comparing Figures 2 and 5, we note that
 602 the largest percentage gains in streamflow occur in watersheds at low- to mid-elevations on the
 603 west slope of the Sierra Nevada where the forest is initially dense and precipitation is relatively
 604 low. In this relatively arid zone, pre-restoration streamflow generation is low, so small changes
 605 to the water balance can lead to large percentage streamflow gains. Considering absolute
 606 differences in area-normalized streamflow instead of percentage differences, forest restoration
 607 has the largest effect in sub-watersheds with a combination of relatively high precipitation and
 608 dense pre-restoration forests. Most of the landscape-scale increase in water yield is

609 attributable to forest disturbance in relatively wet regions, but the largest relative impact on
610 streamflow generation occurs in relatively dry regions.

611 3.5 Simulated Effects on Water Balance Partitioning

612 Precipitation inputs to DHSVM are identical in all management scenarios, so changes in
613 other water balance terms must sum to zero. Calculating the difference in water balance fluxes
614 between forest management scenarios reveals the impact of forest restoration on water
615 balance partitioning. Yearly storage changes and soil evaporation only show negligible
616 differences between management scenarios, so these terms are excluded from comparison
617 here. The negligible change in simulated soil evaporation is partially a result of our assumption
618 that light understory is present in all forested grid cells (Section 2.1).

619 Systematic increases in water yield from forest restoration are primarily attributable to
620 decreased canopy interception loss, because increases in understory transpiration largely
621 compensate for decreases in overstory transpiration (Figure 6). For the remainder of this
622 section, analogous numeric values are given first for the wetter future climate (CNRM-CM5)
623 and second for the drier future climate (MIROC5). Mean overstory transpiration is 42 or 40
624 mm/yr lower on average across all years in the full restoration scenario relative to business-as-
625 usual. However, mean annual understory transpiration is 31 or 29 mm/yr higher in the full
626 restoration scenario, which compensates for 72% or 73% of the reduction in overstory
627 transpiration. Mean interception loss from the canopy is 41 or 35 mm/yr lower in the full
628 restoration scenario, while understory interception loss increases by only 9 or 7 mm/yr, a
629 smaller compensation of 21% in both climates. Since increases in understory ET do not fully
630 compensate for decreases in overstory ET, the full restoration scenario generates 45 or 40
631 mm/yr more streamflow on average relative to the business-as-usual scenario. About 27% or
632 28% of the increased streamflow generation in the full restoration scenario is attributable to
633 decreased transpiration and about 73% or 72% of increased streamflow generation is
634 attributable to decreased interception loss.



635

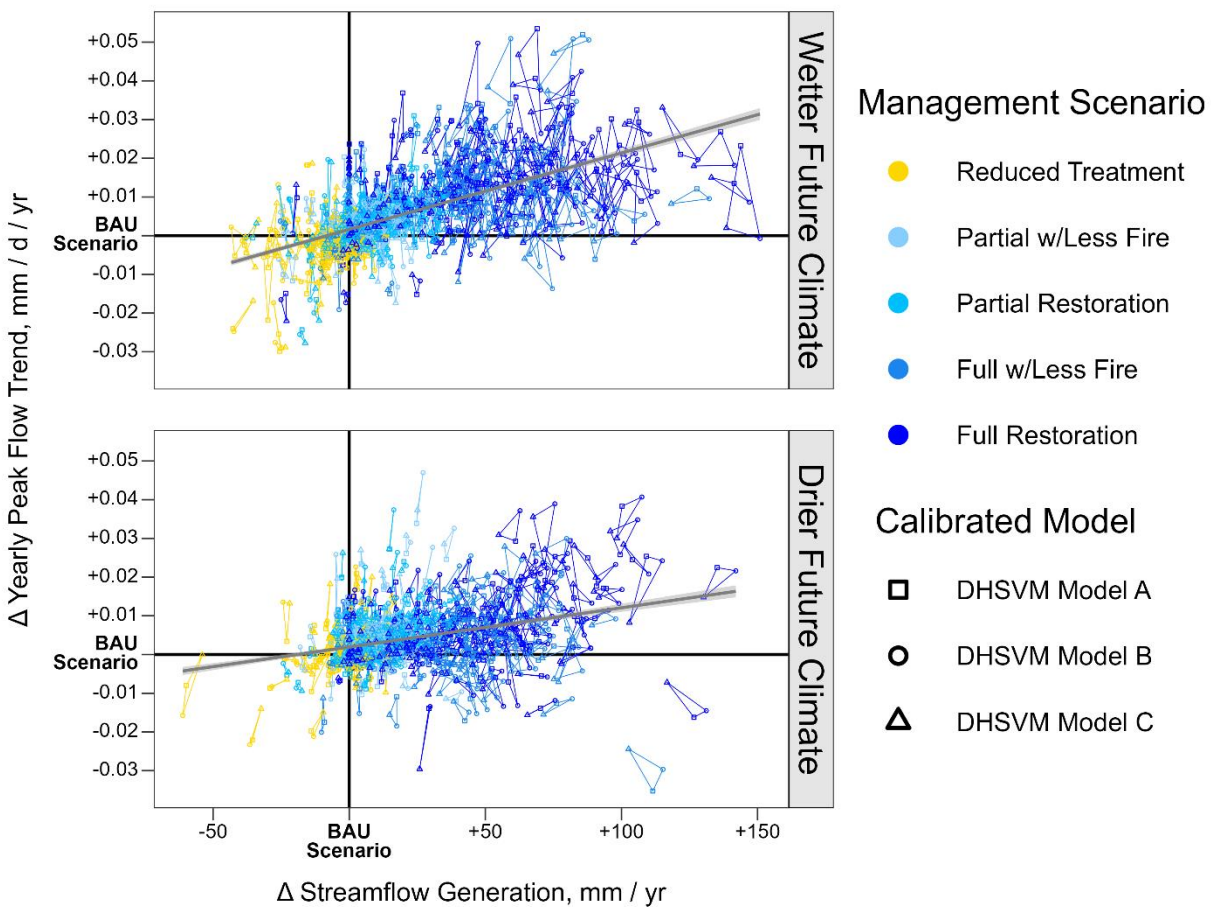
636 **Figure 6.** Timeseries of differences in yearly water balance fluxes between full restoration (S6)
 637 and business-as-usual (BAU, S2) forest management scenarios, averaged across the entire study
 638 area. All terms are calculated as the difference between forest management scenarios with
 639 equal precipitation, so all changes in the water balance fluxes visualized here approximately
 640 sum to zero each year. Fluxes that are larger component of the water balance in S6 relative to
 641 S2 are positive here, and vice versa. Dashed vertical lines indicate dates where vegetation maps
 642 in DHSVM are updated using outputs from LANDIS-II.

643

3.6 Simulated Effects on Peak Flows

644 DHSVM predicts a trend toward relatively higher one-day yearly peak flows in sub-
 645 watersheds that are subject to a more frequent forest disturbance regime. Both the CNRM-
 646 CM5 and MIROC5 climate projections cause trends towards higher peak flows in at least half of
 647 the 139 sub-watersheds in the project area, calculated as the Sen's slope of one-day yearly
 648 peak flows. The peak flow trend is stronger in the relatively wet CNRM-CM5 climate, with a
 649 median sub-watershed peak flow trend of +0.75% per year in the business-as-usual
 650 management scenario. The analogous median trend in the drier MIROC5 climate is +0.33% per
 651 year. In both climates, scenarios with a more frequent forest disturbance return interval can
 652 produce hydrographs with accelerated peak flow trends in certain sub-watersheds (SI Figure

653 S18). Relative to business-as-usual (S2), yearly one-day peak flows in the full restoration
 654 scenario (S6) are 3% or 6% higher on average across all sub-watersheds in the wetter and drier
 655 climates, respectively. There is a large degree of variation in the relative sub-watershed peak
 656 flow response (SI Figure S19), and the maximum difference between mean annual peak flows
 657 for particular sub-watersheds in these two scenarios is as high as 23% in the wetter climate or
 658 39% in the drier climate. However, percentage-based metrics can overemphasize sub-
 659 watersheds with relatively low streamflow, so it is more informative to compare Sen's slope
 660 trends in area-normalized specific discharge units (mm/d/yr), as in Figure 7. Note that the
 661 streamflow generation effect is calculated after subtracting upstream watershed contributions,
 662 but the peak flow trend is calculated from raw hydrographs to represent the actual peak flows
 663 in a particular channel reach (including upstream contributions).

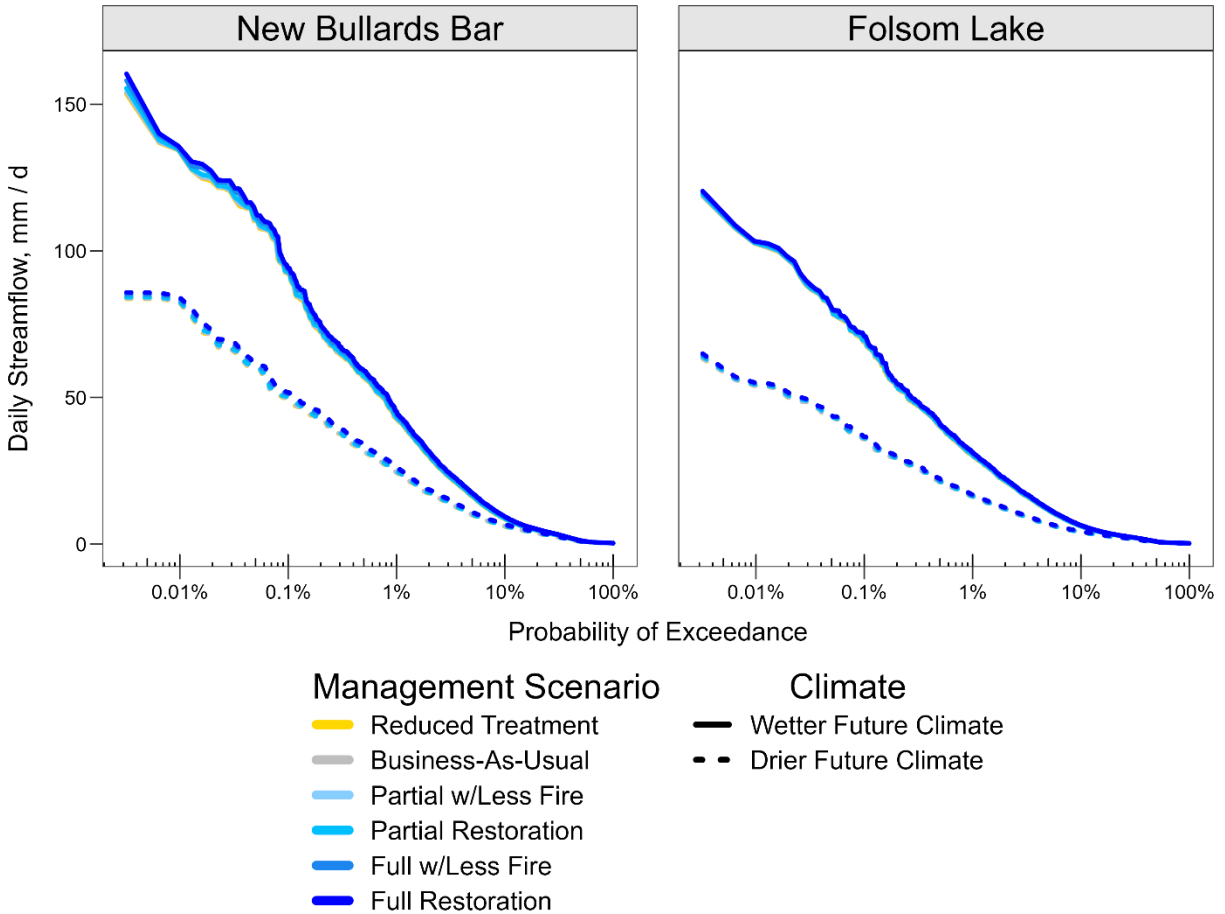


664

665 **Figure 7.** Relationship between increased streamflow generation and increased one-day yearly
 666 peak flows for sub-watersheds subject to different forest restoration scenarios. Differences in
 667 streamflow generation and peak flow trend are shown for the full-restoration scenario (S6)
 668 relative to the business-as-usual (BAU, S2) scenario. Each point represents a single sub-
 669 watershed simulated with a particular DHSVM model. The results from all three calibrated
 670 DHSVM models are connected with line segments, creating a triangular region that represents
 671 the uncertainty in the response of each sub-watershed.

672 We observe a tradeoff between increased streamflow generation and elevated peak
673 flow trends in scenarios with more frequent forest disturbance (Figure 7). Considering all sub-
674 watersheds across all management scenarios, the correlation between additional water yield
675 and a higher peak flow trend is stronger in the wetter future climate ($r = 0.60$ in CNRM-CM5
676 and $r = 0.33$ in MIROC5). Relative to the business-as-usual scenario (S2) and averaged across all
677 three models, both climates, and all 139 sub-watersheds (area-weighted), the reduced
678 treatment scenario (S1) has 2 mm/yr less streamflow generation and no clear pattern of peak
679 flow change. The scenarios with partial restoration of the disturbance return interval have
680 increased streamflow generation of 8 mm/yr (S3, less fire) or 9 mm/yr (S4, more fire), with peak
681 flow trends higher by 0.0036 mm/d/yr (S3) or 0.0037 mm/d/yr (S4). Finally, full restoration of
682 the disturbance return interval produces increased streamflow generation of 34 mm/yr (S5, less
683 fire) or 42 mm/yr (S6, more fire), with peak flow trends higher by 0.0062 mm/d/yr (S5) or
684 0.0094 mm/d/yr (S6). Compared to the partial restoration scenarios (S3 and S4), the full
685 restoration scenarios (S5 and S6) are about 4.5 times as efficacious at producing additional
686 streamflow.

687 At watershed scales that are relevant for reservoir operations, the effect of forest
688 restoration on peak flows is overwhelmed by the uncertainty of future climate projections.
689 There are two major artificial reservoirs in the project domain: New Bullards Bar (capacity
690 966,00 acre-ft. / 1.19 km³) in the North Yuba River watershed, and Folsom Lake (capacity
691 976,000 acre-ft. / 1.20 km³) at the outlet of the American River watershed. Comparing daily
692 flow duration curves for both of these reservoirs derived from DHSVM shows that forest
693 management only has potential to exert a negligible impact on the high flow regime compared
694 to the uncertainty in future precipitation trends (Figure 8). We note that the reservoir-scale
695 peak flow statistics presented here are calculated from raw modeled hydrographs, not
696 accounting for upstream diversions or artificial storage, and are thus not suitable for
697 comparison with historical flow records. Over all 85 years in the simulation period, the mean
698 yearly one-day peak flow is 80% higher for New Bullards Bar and 94% higher for Folsom Lake in
699 CNRM-CM5 compared to MIROC5. Comparing the same statistic between full restoration (S6)
700 and business-as-usual (S2) scenarios, the mean yearly one-day peak flow increases by 4% or 7%
701 for New Bullards Bar and 4% or 6% for Folsom Lake in the CNRM-CM5 and MIROC5 climates,
702 respectively. Thus, uncertainty in the future climate is about 14 times or 20 times larger than
703 the potential impact of forest thinning on annual peak flows into New Bullards Bar and Folsom
704 Lake, respectively.



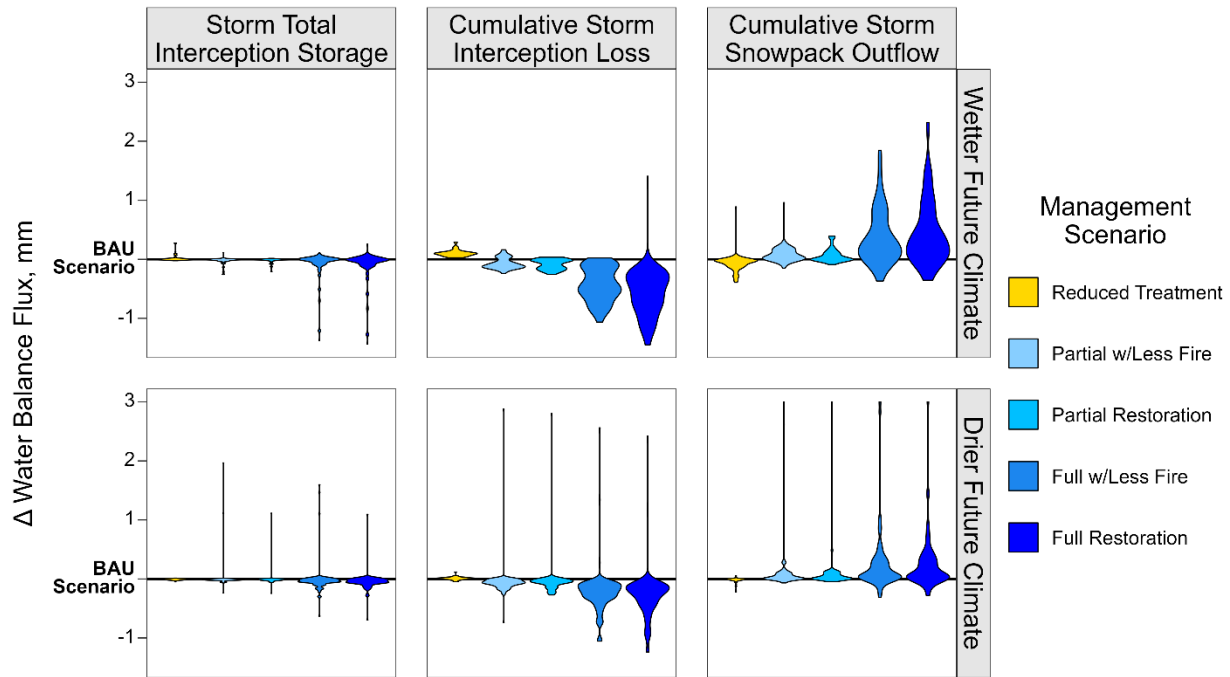
705

706 **Figure 8.** Flow duration curves for two major reservoirs in the project area, calculated using
 707 daily natural (unregulated) inflows simulated by DHSVM for the full 85-year period. Note the
 708 large difference in the high flow regime between climate models compared to the small
 709 difference in high flows between forest restoration scenarios. The probability of exceedance is
 710 logarithmically scaled to emphasize variations in the high flow regime.

711 **3.7 Simulated Effects on Hydrological Processes During Major Storms**

712 In scenarios with a thinner forest canopy, decreased interception and increased
 713 snowmelt may both contribute to increased runoff during major storms (Figure 9). As discussed
 714 in Section 2.3, we define the 10 highest-intensity storms immediately preceding yearly peak
 715 flow events in each of the four main watersheds for all three DHSVM models, thus identifying
 716 120 storm runoff simulations in each scenario for each climate projection. In scenarios with a
 717 thinner forest canopy, interception is generally decreased while snowpack outflow is generally
 718 increased during these storm runoff periods, although some combinations of watershed and
 719 hydrological model produce outlying results for certain storms. In our simulations, forest
 720 restoration has a larger effect on cumulative storm-total interception vapor loss compared to
 721 net storm-total interception storage, because the same storage capacity may be filled and
 722 evaporated repeatedly during multi-day storms. Snowpack outflow from DHSVM includes both

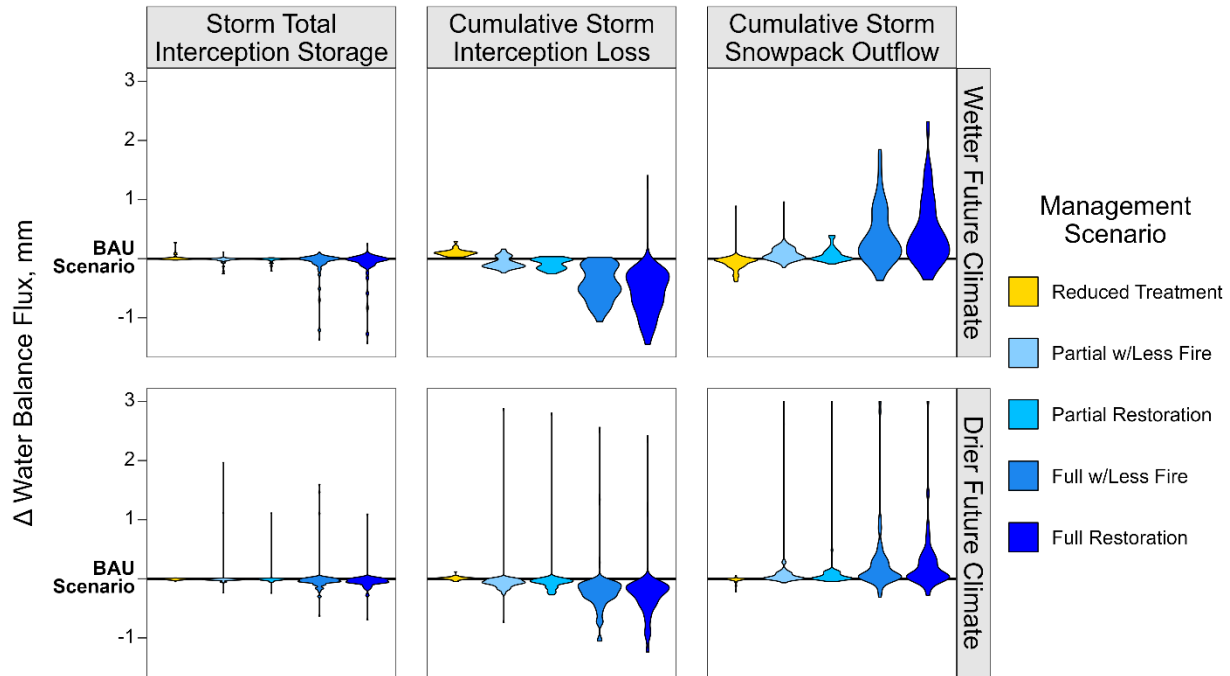
723 snowmelt and rain percolation, so some or all of the increased snowpack outflow in scenarios
 724 with a thinner canopy may be attributable to increased rain throughfall caused by reduced
 725 canopy interception.



726

727 **Figure 9.** Forest restoration effect on storm-total interception storage, storm-total cumulative
 728 interception loss, and storm-total snowpack outflow during intense precipitation events prior to
 729 yearly peak flows, calculated as a landscape average for each of four major watersheds
 730 simulated by each of three DHSVM models. Results are shown for the full-restoration scenario
 731 (S6) relative to the business-as-usual (BAU, S2) scenario.

732 During storm events associated with yearly peak flows, the effect of a thinner forest
 733 canopy on the snowpack energy balance varies in space and time. In scenarios with a thinner
 734 forest canopy, the snowpack generally receives increased shortwave radiation, increased
 735 advected energy (from precipitation throughfall), and decreased longwave radiation (Figure
 736 10). However, as a result of differing positive or negative signs between the shortwave,
 737 longwave, and advected energy effects, the net snowpack energy budget in a thinner forest
 738 may increase or decrease depending on the specific circumstances of each storm. Simulated
 739 sensible and latent heat fluxes do not show a clear pattern of change. We note that the small
 740 magnitude of energy balance changes in Figure 10 (on the order of 1 W/m^2) are area-averaged
 741 values for the entire TCSI area, while snow may exist only in limited areas during these storm
 742 events, especially in later decades. Thus, Figure 10 quantifies relative patterns of change but
 743 does not represent the absolute magnitude of changes to the snowpack energy balance.



744

745 **Figure 10.** Forest restoration effects on the landscape-average snowpack energy balance during
 746 intense precipitation events prior to yearly peak flow events in each of four major watersheds
 747 simulated by each of three DHSVM models relative to the business-as-usual scenario.

748 **3.8 Uncertainty in Sub-Watershed Streamflow Responses**

749 The uncertainty of the calibrated hydrological model ensemble is considerably smaller
 750 than both the average magnitude and spatial heterogeneity of the predicted streamflow
 751 generation effects. In Figure 5, which shows the additional streamflow generation attributable
 752 to forest restoration, analogous results from all three selected DHSVM models are interwoven
 753 using a checkerboard pattern, where every third square is representative of the value from a
 754 single calibrated model. The resolution of the checkerboard is selected for ease of visualization,
 755 and the actual grid size of DHSVM is much smaller (90 m). Greater uniformity in the
 756 checkerboard pattern indicates proportionally lower uncertainty in the hydrological model
 757 ensemble. Overall, the uncertainty between different DHSVM ensemble members is about an
 758 order of magnitude smaller than the size of the predicted effects attributable to forest
 759 management.

760 The peak flow response to forest thinning is more uncertain than the streamflow
 761 generation response, but both responses show significant patterns of spatial heterogeneity. In
 762 Figure 6, hydrological model uncertainty is visualized with triangles defined by the results from
 763 all three calibrated DHSVM models in each sub-watershed. Although the true response of a
 764 given sub-watershed could fall outside the bounds of its modeled range (enclosed triangle), the
 765 overall spread of the three ensemble members gives an estimate of model uncertainty. In the
 766 full restoration (S6) scenario relative to business-as-usual (S2), the sub-watershed streamflow
 767 generation response has an average model uncertainty range of 5.3 mm/yr among the three

768 DHSVM models and an average difference of 7.9 mm/yr between both climate models. The
769 mean sub-watershed streamflow response to forest restoration (S6 vs. S2) is 44 mm/yr with a
770 standard deviation among sub-watersheds of 32 mm/yr. Analogously, the S6 vs. S2 peak flow
771 trend difference in each sub-watershed varies by 0.0075 mm/d/yr on average among DHSVM
772 models and 0.0090 mm/d/yr on average between climates, with a mean across sub-watersheds
773 of 0.0097 mm/d/yr and a standard deviation among sub-watersheds of 0.0083 mm/d/yr. For
774 most sub-watersheds, the magnitude of the predicted streamflow generation response
775 considerably outweighs both the uncertainty of the model (~12%) and the mediating effect of
776 climate (~18%), but the peak flow response has much higher model uncertainty (~78%) and
777 much greater dependence on climate mediation (~93%). Nevertheless, we observe that the
778 largest sub-watershed peak flow responses are relatively well-constrained based on the
779 individual confidence regions in Figure 6. The maximum response for any one sub-watershed
780 averaged across models and climates is 140 mm/yr of additional streamflow generation or a
781 0.037 mm/d/yr higher peak flow trend. Thus, locally strong sub-watershed responses are well-
782 resolved relative to the model uncertainty.

783 3.9 Uncertainty in Reservoir-Scale Water Yield

784 Despite uncertainty in the future climate, the absolute magnitude of additional water
785 yield into reservoirs under different forest restoration scenarios is well-constrained. Here, we
786 consider mean yearly runoff into each reservoir over the full 85-year simulation period in the
787 full restoration scenario (S6) relative to the business-as-usual scenario (S2). For the New
788 Bullards Bar watershed, DHSVM predicts an additional 99,800 acre-ft/yr (0.123 km^3) of yearly
789 runoff in the wetter CNRM-CM5 climate or an additional 90,700 acre-ft/yr (0.112 km^3) of yearly
790 runoff in the drier MIROC5 climate. For Folsom Lake, the additional inflow is 176,000 acre-ft/yr
791 (0.217 km^3) under CNRM-CM5 or 158,000 acre-ft/yr (0.195 km^3) under MIROC5. The total mean
792 annual runoff between wetter and drier climate projections varies by 46% for New Bullards Bar
793 and 55% for Folsom Lake, but the volume of additional runoff attributable to forest restoration
794 varies by only 10% or 12% between climates for the same reservoirs. Thus, the additional water
795 yield from forest restoration is about five times less sensitive to uncertainty in future
796 precipitation trends compared to the total future water yield (46% vs. 10% uncertainty for New
797 Bullards Bar and 55% vs. 12% uncertainty for Folsom Lake).

798 The relative contribution of additional runoff from forest restoration as a percentage of
799 the total yearly volume is dependent on future climate trends and interannual variability.
800 Relative to the business-as-usual scenario, additional water yield from the full restoration
801 scenario amounts to 7% or 9% of the mean annual inflow for New Bullards Bar and 4% or 6% for
802 Folsom Lake in the wetter or drier climate projections, respectively. Considering only the 10
803 driest years (by annual precipitation), the absolute additional runoff in the full restoration
804 scenario relative to business-as-usual is 71,900 acre-ft/yr (0.0887 km^3) or 52,300 acre-ft/yr
805 (0.0645 km^3) for New Bullards Bar and 113,000 acre-ft/yr (0.139 km^3) or 78,400 acre-ft/yr
806 (0.0967 km^3) for Folsom Lake in the wetter and drier climate projections, respectively. This
807 additional runoff amounts to 12% or 14% of the total annual inflow for New Bullards Bar and
808 8% or 9% of the total annual inflow for Folsom Lake during the same 10 driest years, again in

809 the wetter or drier climates. While the absolute volume of additional water yield attributable to
810 forest restoration decreases during dry climate conditions, the percent difference between
811 business-as-usual and full restoration scenarios increases. Therefore, forest restoration would
812 have the largest relative impact on reservoir-scale water yield during drought years, particularly
813 in a drier climate.

814 **4 Discussion**

815 **4.1 Reservoir-Scale Drought Hedge**

816 Our results suggest that increased water yields from landscape-scale forest restoration
817 can provide a hedge against future droughts in the central Sierra Nevada region, on the order of
818 8-14% increases in reservoir water yield during dry years. Compared to the annual water yield,
819 streamflow gains from forest restoration are about five times less sensitive to uncertainty in the
820 annual precipitation volume. This reduced sensitivity of streamflow gains follows from the
821 partial decoupling of precipitation and forest ET in the relatively energy-limited study region, as
822 previously shown by Saksa et al. (2017) for the same geographic area. This result is
823 hydrologically intuitive because the impact of forest thinning is bounded by the maximum
824 interception loss and transpiration rates supported by the initial forest. For example, trees have
825 a minimum stomatal resistance beyond which additional soil moisture does not increase
826 transpiration rates. Similarly, once interception storage becomes saturated during a storm,
827 additional precipitation is less affected by canopy structure. From a management perspective,
828 the environmental and economic value of additional streamflow generated from a thinner
829 forest is likely to be contingent upon trends in future precipitation (see Guo et al. 2023 for a
830 discussion of the marginal price of water in the study region). Even in a wetter future climate,
831 certain years will likely still qualify as droughts, and the partial decoupling of additional runoff
832 from precipitation could benefit the water supply in those dry years. Thus, the value
833 proposition of forest restoration for water resources in the central Sierra Nevada region may
834 best be understood as a hedge against a possible drier future climate and/or drought years in
835 any future climate.

836 The magnitude of additional water yield from forest restoration as predicted by DHSVM
837 is generally supported by prior findings in similar environments. In a small sub-basin of the
838 American River watershed, included in our study area, Saksa et al. (2017) used a combination of
839 process-based modeling and field data to estimate a 14% increase in streamflow generation
840 after forest thinning. While a direct comparison is not possible due to differences in scale and
841 treatment intensity, the empirical findings of Saksa et al. (2017) align with our model results in
842 the same geographic region (Figure 5). Using statistical approaches based on relationships
843 between measured ET and maps of the normalized difference vegetation index (NDVI) from
844 remote sensing, Roche et al. (2020) estimated a 150-200 mm/yr potential streamflow gain from
845 forest fires or thinning in the American and Yuba River watersheds. This streamflow gain is
846 larger than predicted by our simulation for almost all sub-watersheds (Figure 7). While
847 individual fires might cause extreme changes in the local water balance, our results indicate
848 that it would be overly optimistic to expect such a large streamflow response from forest

849 restoration at the landscape or even sub-watershed scale. Similarly, Guo et al. (2023) estimate
850 reductions in ET as high as 361-371 mm/yr for high-severity wildfire or 269-277 mm/yr for
851 medium-severity wildfire for small forest treatment areas (15.6-23.1 km²) at the headwaters of
852 the Yuba and American watersheds. Our results similarly suggest that these high ET reductions
853 are unlikely to be realized from forest restoration at larger landscape scales, and we estimate a
854 mean landscape ET reduction (overstory and understory transpiration plus interception loss) of
855 only 41 mm/yr in the full restoration scenario. Nevertheless, extrapolation of empirical NDVI-
856 based methods can produce similar water yield results at the landscape scale, provided that
857 enough recent fires have occurred in the region of interest to constrain variable vegetation
858 responses to disturbance: in the American River watershed, Roche et al. (2018) estimate a 5%
859 (all years) or 10% (dry years) increase in reservoir inflow under a restored disturbance regime,
860 remarkably close to the increase of 4-6% (all years) and 8-9% (10 driest years) modeled for the
861 same basin in this study.

862 4.2 Sub-Watershed Heterogeneity

863 The additional water yield from forest restoration could be maximized by targeting
864 treatments to sub-watersheds with particularly dense forests and high average precipitation.
865 Forest management planning could prioritize mechanical thinning and prescribed fire in sub-
866 watersheds with the greatest potential for increased streamflow generation (Figure 5).
867 Additionally, a machine learning model such as Random Forest could potentially be trained on
868 the process-based DHSVM results in a meta-model decision support framework (Mijic et al.
869 2024), such as the tool implemented by Lewis et al. (2023) for the snowpack response to forest
870 restoration in the same geographical region. Other studies have demonstrated the ranges of
871 forest density and canopy gap size that can best promote snow accumulation (Piske et al., in
872 press), but these fine scales are not explored in the present study. With knowledge of the
873 potential tradeoff between increased streamflow generation and higher peak flow trends
874 (Figure 7), it may be desirable to target forest restoration in sub-watersheds that balance the
875 utility of additional water yield against the risk of damage to small-scale infrastructure from
876 high flows. In the TCSI region, the elevation head and capacity of downstream hydroelectric
877 plants further mediates the potential benefit of additional streamflow generation (Guo et al.
878 2023). From a water resources perspective, the ideal areas for forest restoration could be dense
879 forests that are situated above power-generating reservoirs, since these reservoirs can benefit
880 from increased inflow and mediate increases in peak flows.

881 Although forest restoration may cause locally higher peak flows, any significant impacts
882 are limited to headwaters and are unlikely to affect reservoir operations. DHSVM predicts peak
883 flow increases on the order of 10-30% in certain sub-watersheds, but these are small
884 headwaters catchments with relatively low absolute streamflow magnitudes, on the order of
885 0.1 to 10 m³/s (SI Figure S20). Increases in small-scale peak flows could accentuate risks to
886 hydraulic infrastructure such as road culverts, many of which are only engineered for 25-year
887 peak flows and are now aging and vulnerable to washouts (Halofsky et al. 2021). Additionally,
888 elevated surface runoff in headwaters regions could exacerbate erosion and sediment loading
889 from historic hydraulic mining sites, which are prevalent in the study area (Gilbert 1917 and

890 Curtis et al. 2005). The effect of forest restoration on peak flows attenuates rapidly at larger
891 scales, and reservoir operations are unlikely to be significantly impacted by landscape-scale
892 forest restoration in the central Sierra Nevada region. One key uncertainty in our results is the
893 lack of changes in the DHSVM soil and snow properties that could contribute to faster runoff or
894 faster snowmelt, such as increased soil hydrophobicity (Certini 2005) or darkened snow albedo
895 from pyrogenic carbon (e.g., Gleason et al. 2013). Because uncertain future precipitation trends
896 almost exclusively control the high flow regime, flood management planning will likely become
897 increasingly motivated by the potential for extreme precipitation and rapid snowmelt events
898 (Harpold and Kohler 2017, Hou et al. 2019). For example, a project is currently planned to add a
899 second spillway to the New Bullards Bar Reservoir to reduce flood risk associated with
900 atmospheric river storms (Yuba Water Agency 2023).

901 4.3 Overstory-Understory Compensation

902 A process-based modeling approach is necessary to untangle the compensating
903 responses of overstory and understory vegetation to forest restoration. Reduced canopy
904 interception can lead to greater terrestrial water input (rain + snowmelt), and lower overstory
905 transpiration can lead to higher soil moisture. Not all excess terrestrial water input necessarily
906 becomes streamflow though, as noted empirically after widespread insect-driven forest
907 mortality (e.g., Biederman et al. 2015). Wetter soil and reduced canopy shading can both
908 contribute to increases in ET from remaining vegetation and soil evaporation (Boisramé et al.
909 2019). Moreover, elevated soil moisture may encourage regrowth of both understory and
910 trees, so continued treatment by mechanical thinning or fire is necessary to maintain a thinner
911 forest state, as implemented in the scenarios tested here (Maxwell et al. 2022).

912 We observe a strong compensation between overstory and understory transpiration in
913 addition to a weaker tradeoff between overstory and understory interception loss (Figure 6).
914 Neglecting increases in understory ET during forest restoration would lead to about an 86%
915 overestimation of the predicted streamflow response. About 73% of the streamflow response
916 that we do predict is attributable to reductions in canopy interception loss. Understory
917 interception has only a limited capacity for compensation due to lower height and the
918 sheltering effect of remaining trees, both of which contribute to limitations on solar insolation
919 and turbulent vapor transport. Additionally, DHSVM assumes that understory is buried when
920 snow is present in a grid cell, so cold-season precipitation can only be intercepted by the
921 overstory canopy. One limitation of our approach is that the understory maps in DHSVM are
922 updated using a regression model coupled to the LANDIS-II outputs instead of by direct
923 simulation of shrub and herb communities in LANDIS-II. Our results show the importance of
924 improving simulations of multiple vegetation layers and understory regrowth to better
925 constrain compensating ET effects following forest disturbance.

926 4.4 Uncertainty

927 A model ensemble derived from multi-objective Bayesian calibration enables the
928 propagation of model parameter uncertainty into our analysis of hydrological responses to
929 forest restoration. The structure of fully distributed, process-based models like DHSVM is well-

930 suited for extrapolating hydrological interactions to spatially heterogeneous vegetation and
931 climate conditions outside the range of historical observations. However, process-based
932 hydrological models are typically deterministic and challenging to fully constrain with
933 observational data, making uncertainty quantification difficult and threatening the integrity of
934 predictions (e.g., Beven 1993). By applying a multi-objective Bayesian calibration and selecting
935 an ensemble of Pareto-efficient parameter sets, we are able to estimate model uncertainty and
936 propagate it into our final results (Figures 5 and 7). Despite considerable uncertainty remaining
937 in landscape-scale subsurface parameters (e.g., soil depth and porosity), differences in
938 ensemble model predictions at the sub-watershed scale are roughly an order of magnitude
939 smaller than the size of streamflow generation effects attributable to forest restoration.

940 Not all forms of uncertainty can be explicitly represented in our model calibration, and
941 we choose to focus on key processes and parameters identified as sensitive in previous DHSVM
942 studies (e.g., Du et al. 2014). Although our conclusions are robust across two GCMs that are
943 endmembers of fire weather (Maxwell et al. 2022), both GCMs are downscaled using the same
944 MACA technique (Abatzoglou and Brown 2012), which may lead to underestimation of future
945 climate uncertainty (Alder and Hostetler 2018). The MACA downscaling technique, which is
946 based on historical analogues, also may not fully capture the dynamics of future atmospheric
947 river storms (e.g., Gershunov et al. 2019, Huang et al. 2020). There is also the possibility of
948 unforeseen “black swan” events like invasive insects or megafires that could drastically alter the
949 trajectory of forest ecosystems outside the LANDIS-II simulation scope. Despite these modeling
950 limitations, the consistency of our water balance results across multiple calibrated parameter
951 sets and future climate projections should increase confidence in the potential water resource
952 impacts of central Sierra Nevada forest restoration scenarios.

953 **5 Conclusions**

954 Landscape-scale forest restoration shows promise as a hedge against future droughts. In
955 the central Sierra Nevada mountains, distributed hydrological modeling predicts that full
956 restoration of the historic disturbance return interval could produce 8-14% more inflow into
957 major reservoirs during dry years. Increased streamflow can benefit aquatic and riparian
958 ecosystems, hydropower operations, and municipal or agricultural water customers. In the
959 context of recent Sierra Nevada multi-year droughts (e.g., 2013-2015 and 2020-2022), these
960 benefits may help incentivize investment in central Sierra Nevada forest restoration. Despite
961 considerable climate-driven uncertainty in the total future water supply (46-55%), the effect of
962 forest restoration on water yield is relatively well-constrained. In the relatively energy-limited
963 central Sierra Nevada hydroclimate, streamflow gains from forest restoration are partially
964 decoupled from yearly precipitation. Combined with the higher value of water in dry years, this
965 reduced climate sensitivity enhances the value of forest restoration as a potential drought
966 hedge. In a thinner forest, reduced canopy interception and increased snowpack outflow during
967 major storms can increase peak flows in headwaters catchments, but this risk is effectively
968 limited to the scale of smaller road culverts rather than reservoirs. Densely forested sub-
969 watersheds immediately upstream of reservoirs appear most favorable for targeted forest
970 restoration due to the tradeoff between increased water yield and higher peak flows.

971 Our study demonstrates the value of linking process-based ecosystem and hydrological
972 models to predict the water resource impacts of landscape-scale forest restoration. However,
973 extrapolating our results across the western U.S., or even across the Sierra Nevada mountains,
974 is challenging due to the mediating role of aridity, forest type, land cover history, and other
975 factors. Applying similar methods across a wider range of regional climates and forest
976 conditions may help constrain the sensitivity of our results and help prioritize forest restoration
977 priorities.

978 **Acknowledgments**

979 This work was supported by funding from the USDA Forest Service Pacific Southwest Research
980 Station. A. A. Harpold and E. N. Boardman were partially supported by NSF EAR #2012310 and
981 EAR #1723990. E. N. Boardman was additionally supported by the NSF Graduate Research
982 Fellowship Program under Grant #1937966.

983 **Availability Statement**

984 DHSVM and LANDIS-II are both open-source models, with ongoing development by the Pacific
985 Northwest National Laboratory (<https://github.com/pnnl/DHSVM-PNNL>) and the LANDIS-II
986 Foundation (<https://github.com/LANDIS-II-Foundation>), respectively. Code related to the
987 hydrological modeling for this project is available at [https://github.com/eli-mtnhydro/TCSI-](https://github.com/eli-mtnhydro/TCSI-ForestHydrology)
988 [ForestHydrology](https://github.com/eli-mtnhydro/TCSI-ForestHydrology). Code related to the forest ecosystem modeling for this project is available at
989 <https://github.com/LANDIS-II-Foundation/Project-Tahoe-Central-Sierra-2019>. The model
990 inputs, outputs, processed results, and other data needed to recreate the results and figures in
991 this study are archived at <https://doi.org/10.5281/zenodo.13984265>.

992

993 **References**

- 994 Abatzoglou, J. T. (2013). Development of gridded surface meteorological data for ecological
995 applications and modelling. *International Journal of Climatology*, 33(1), 121–131.
996 <https://doi.org/10.1002/joc.3413>
- 997 Abatzoglou, J. T., & Brown, T. J. (2012). A comparison of statistical downscaling methods suited
998 for wildfire applications. *International Journal of Climatology*, 32(5), 772–780.
999 <https://doi.org/10.1002/joc.2312>
- 1000 Adams, H. D., Luce, C. H., Breshears, D. D., Allen, C. D., Weiler, M., Hale, V. C., Smith, A. M. S., &
1001 Huxman, T. E. (2012). Ecohydrological consequences of drought- and infestation-
1002 triggered tree die-off: Insights and hypotheses. *Ecohydrology*, 5(2), 145–159.
1003 <https://doi.org/10.1002/eco.233>
- 1004 Alder, J. R., & Hostetler, S. W. (2019). The Dependence of Hydroclimate Projections in Snow-
1005 Dominated Regions of the Western United States on the Choice of Statistically
1006 Downscaled Climate Data. *Water Resources Research*, 55(3), 2279–2300.
1007 <https://doi.org/10.1029/2018WR023458>
- 1008 Andréassian, V. (2004). Waters and forests: From historical controversy to scientific debate.
1009 *Journal of Hydrology*, 291(1), 1–27. <https://doi.org/10.1016/j.jhydrol.2003.12.015>
- 1010 Bales, R. C., Goulden, M. L., Hunsaker, C. T., Conklin, M. H., Hartsough, P. C., O’Geen, A. T.,
1011 Hopmans, J. W., & Safeeq, M. (2018). Mechanisms controlling the impact of multi-year
1012 drought on mountain hydrology. *Scientific Reports*, 8(1), 690.
1013 <https://doi.org/10.1038/s41598-017-19007-0>
- 1014 Bales, R. C., Molotch, N. P., Painter, T. H., Dettinger, M. D., Rice, R., & Dozier, J. (2006).
1015 Mountain hydrology of the western United States. *Water Resources Research*, 42(8).
1016 <https://doi.org/10.1029/2005WR004387>
- 1017 Beckers, J., Smerdon, B., & Wilson, M. (2009). Review of hydrologic models for forest
1018 management and climate change applications in British Columbia and Alberta. *FORREX*
1019 *Forum for Research and Extension in Natural Resources*, Series 25.
- 1020 Bennett, A., Hamman, J., & Nijssen, B. (2020). MetSim: A Python package for estimation and
1021 disaggregation of meteorological data. *Journal of Open Source Software*, 5(47), 2042.
1022 <https://doi.org/10.21105/joss.02042>
- 1023 Beven, K. (1993). Prophecy, reality and uncertainty in distributed hydrological modelling.
1024 *Advances in Water Resources*, 16(1), 41–51. [https://doi.org/10.1016/0309-](https://doi.org/10.1016/0309-1708(93)90028-E)
1025 [1708\(93\)90028-E](https://doi.org/10.1016/0309-1708(93)90028-E)
- 1026 Biederman, J. A., Harpold, A. A., Gochis, D. J., Ewers, B. E., Reed, D. E., Papuga, S. A., & Brooks,
1027 P. D. (2014). Increased evaporation following widespread tree mortality limits

- 1028 streamflow response. *Water Resources Research*, 50(7), 5395–5409.
 1029 <https://doi.org/10.1002/2013WR014994>
- 1030 Biederman, J. A., Somor, A. J., Harpold, A. A., Gutmann, E. D., Breshears, D. D., Troch, P. A.,
 1031 Gochis, D. J., Scott, R. L., Meddens, A. J. H., & Brooks, P. D. (2015). Recent tree die-off
 1032 has little effect on streamflow in contrast to expected increases from historical studies.
 1033 *Water Resources Research*, 51(12), 9775–9789. <https://doi.org/10.1002/2015WR017401>
- 1034 Binois, M., & Picheny, V. (2019). GPareto: An R Package for Gaussian-Process-Based Multi-
 1035 Objective Optimization and Analysis. *Journal of Statistical Software*, 89(8).
 1036 <https://doi.org/10.18637/jss.v089.i08>
- 1037 Blöschl, G., Bierkens, M. F. P., Chambel, A., Cudennec, C., Destouni, G., Fiori, A., Kirchner, J. W.,
 1038 McDonnell, J. J., Savenije, H. H. G., Sivapalan, M., Stump, C., Toth, E., Volpi, E., Carr, G.,
 1039 Lupton, C., Salinas, J., Széles, B., Viglione, A., Aksoy, H., ... Zhang, Y. (2019). Twenty-three
 1040 unsolved problems in hydrology (UPH) – a community perspective. *Hydrological
 1041 Sciences Journal*, 64(10), 1141–1158. <https://doi.org/10.1080/02626667.2019.1620507>
- 1042 Boardman, E. (2024). Dataset for Water Resource / Forest Restoration Modeling in Tahoe-
 1043 Central Sierra Region [Data set]. Zenodo. <https://doi.org/10.5281/zenodo.13984265>
- 1044 Boisramé, G. F. S., Thompson, S. E., Tague, C. (Naomi), & Stephens, S. L. (2019). Restoring a
 1045 Natural Fire Regime Alters the Water Balance of a Sierra Nevada Catchment. *Water
 1046 Resources Research*, 55(7), 5751–5769. <https://doi.org/10.1029/2018WR024098>
- 1047 Boisramé, G., Thompson, S., Collins, B., & Stephens, S. (2017). Managed Wildfire Effects on
 1048 Forest Resilience and Water in the Sierra Nevada. *Ecosystems*, 20(4), 717–732.
 1049 <https://doi.org/10.1007/s10021-016-0048-1>
- 1050 Boisramé, G., Thompson, S., & Stephens, S. (2018). Hydrologic responses to restored wildfire
 1051 regimes revealed by soil moisture-vegetation relationships. *Advances in Water
 1052 Resources*, 112, 124–146. <https://doi.org/10.1016/j.advwatres.2017.12.009>
- 1053 Boon, S. (2012). Snow accumulation following forest disturbance. *Ecohydrology*, 5(3), 279–285.
 1054 <https://doi.org/10.1002/eco.212>
- 1055 Bosch, J. M., & Hewlett, J. D. (1982). A review of catchment experiments to determine the
 1056 effect of vegetation changes on water yield and evapotranspiration. *Journal of
 1057 Hydrology*, 55(1), 3–23. [https://doi.org/10.1016/0022-1694\(82\)90117-2](https://doi.org/10.1016/0022-1694(82)90117-2)
- 1058 Bowling, L. C., & Lettenmaier, D. P. (2002). Evaluation of the effects of forest roads on
 1059 streamflow in Hard and Ware Creeks, Washington (Technical Report No. 155; Water
 1060 Resources Series). University of Washington.
- 1061 Burrell, E. A., DiTommaso, A. M., Turner, A. M., Pugh, J. A., Christiansen, S. A., & Conkling, B. L.
 1062 (2021). The forest inventory and analysis database: Database description and user guide

- 1063 [Dataset]. U.S. Department of Agriculture, Forest Service.
1064 [https://research.fs.usda.gov/understory/forest-inventory-and-analysis-database-user-](https://research.fs.usda.gov/understory/forest-inventory-and-analysis-database-user-guide-nfi)
1065 [guide-nfi](https://research.fs.usda.gov/understory/forest-inventory-and-analysis-database-user-guide-nfi)
- 1066 Cabiyo, B., Fried, J. S., Collins, B. M., Stewart, W., Wong, J., & Sanchez, D. L. (2021). Innovative
1067 wood use can enable carbon-beneficial forest management in California. *Proceedings of*
1068 *the National Academy of Sciences*, 118(49), e2019073118.
1069 <https://doi.org/10.1073/pnas.2019073118>
- 1070 California Department of Water Resources. (2022). Database of full natural flow records for the
1071 AMF, NAT, and YRS stations [Dataset]. California Data Exchange Center.
1072 <https://cdec.water.ca.gov/index.html>
- 1073 Cansler, C. A., Hood, S. M., Varner, J. M., Van Mantgem, P. J., Agne, M. C., Andrus, R. A., Ayres,
1074 M. P., Ayres, B. D., Bakker, J. D., Battaglia, M. A., Bentz, B. J., Breece, C. R., Brown, J. K.,
1075 Cluck, D. R., Coleman, T. W., Corace, R. G., Covington, W. W., Cram, D. S., Cronan, J. B., ...
1076 Wright, M. C. (2020). The Fire and Tree Mortality Database, for empirical modeling of
1077 individual tree mortality after fire. *Scientific Data*, 7(1), 194.
1078 <https://doi.org/10.1038/s41597-020-0522-7>
- 1079 Certini, G. (2005). Effects of fire on properties of forest soils: A review. *Oecologia*, 143(1), 1–10.
1080 <https://doi.org/10.1007/s00442-004-1788-8>
- 1081 Chaney, N. W., Minasny, B., Herman, J. D., Nauman, T. W., Brungard, C. W., Morgan, C. L. S.,
1082 McBratney, A. B., Wood, E. F., & Yimam, Y. (2019). POLARIS Soil Properties: 30-m
1083 Probabilistic Maps of Soil Properties Over the Contiguous United States. *Water*
1084 *Resources Research*, 55(4), 2916–2938. <https://doi.org/10.1029/2018WR022797>
- 1085 Chung, M. G., Guo, H., Nyelele, C., Egoh, B. N., Goulden, M. L., Keske, C. M., & Bales, R. C.
1086 (2024). Valuation of forest-management and wildfire disturbance on water and carbon
1087 fluxes in mountain headwaters. *Ecohydrology*, 17(3), e2642.
1088 <https://doi.org/10.1002/eco.2642>
- 1089 Collins, B. M., Everett, R. G., & Stephens, S. L. (2011). Impacts of fire exclusion and recent
1090 managed fire on forest structure in old growth Sierra Nevada mixed-conifer forests.
1091 *Ecosphere*, 2(4), art51. <https://doi.org/10.1890/ES11-00026.1>
- 1092 Cuo, L., Lettenmaier, D. P., Mattheussen, B. V., Storck, P., & Wiley, M. (2008). Hydrologic
1093 prediction for urban watersheds with the Distributed Hydrology-Soil-Vegetation Model.
1094 *Hydrological Processes*, 22(21), 4205–4213. <https://doi.org/10.1002/hyp.7023>
- 1095 Curtis, J. A., Flint, L. E., Alpers, C. N., & Yarnell, S. M. (2005). Conceptual model of sediment
1096 processes in the upper Yuba River watershed, Sierra Nevada, CA. *Geomorphology*, 68(3),
1097 149–166. <https://doi.org/10.1016/j.geomorph.2004.11.019>

- 1098 Dewitz, J., & U.S. Geological Survey. (2019). National Land Cover Database (NLCD) 2019
 1099 Products [Dataset]. U.S. Geological Survey. <https://doi.org/10.5066/P9JZ7A03>
- 1100 Dolanc, C. R., Safford, H. D., Thorne, J. H., & Dobrowski, S. Z. (2014). Changing forest structure
 1101 across the landscape of the Sierra Nevada, CA, USA, since the 1930s. *Ecosphere*, 5(8),
 1102 art101. <https://doi.org/10.1890/ES14-00103.1>
- 1103 Du, E., Link, T. E., Gravelle, J. A., & Hubbart, J. A. (2014). Validation and sensitivity test of the
 1104 distributed hydrology soil-vegetation model (DHSVM) in a forested mountain
 1105 watershed. *Hydrological Processes*, 28(26), 6196–6210.
 1106 <https://doi.org/10.1002/hyp.10110>
- 1107 Dupuy, D., Helbert, C., & Franco, J. (2015). DiceDesign and DiceEval: Two R Packages for Design
 1108 and Analysis of Computer Experiments. *Journal of Statistical Software*, 65, 1–38.
 1109 <https://doi.org/10.18637/jss.v065.i11>
- 1110 Eidenshink, J., Schwind, B., Brewer, K., Zhu, Z.-L., Quayle, B., & Howard, S. (2007). A Project for
 1111 Monitoring Trends in Burn Severity. *Fire Ecology*, 3(1), 3–21.
 1112 <https://doi.org/10.4996/fireecology.0301003>
- 1113 Elias, M., Dees, J., Cabiyo, B., Saksa, P., & Sanchez, D. L. (2023). Financial Analysis of Innovative
 1114 Wood Products and Carbon Finance to Support Forest Restoration in California. *Forest*
 1115 *Products Journal*, 73(1), 31–42. <https://doi.org/10.13073/FPJ-D-22-00049>
- 1116 Ellis, C. R., Pomeroy, J. W., Essery, R. L. H., & Link, T. E. (2011). Effects of needleleaf forest cover
 1117 on radiation and snowmelt dynamics in the Canadian Rocky Mountains. *Canadian*
 1118 *Journal of Forest Research*, 41(3), 608–620. <https://doi.org/10.1139/X10-227>
- 1119 Emmerich, M. T. M., Deutz, A. H., & Klinkenberg, J. W. (2011). Hypervolume-based expected
 1120 improvement: Monotonicity properties and exact computation. 2011 IEEE Congress of
 1121 Evolutionary Computation (CEC), 2147–2154.
 1122 <https://doi.org/10.1109/CEC.2011.5949880>
- 1123 Farr, T. G., Rosen, P. A., Caro, E., Crippen, R., Duren, R., Hensley, S., Kobrick, M., Paller, M.,
 1124 Rodriguez, E., Roth, L., Seal, D., Shaffer, S., Shimada, J., Umland, J., Werner, M., Oskin,
 1125 M., Burbank, D., & Alsdorf, D. (2007). The Shuttle Radar Topography Mission. *Reviews of*
 1126 *Geophysics*, 45(2). <https://doi.org/10.1029/2005RG000183>
- 1127 Gershunov, A., Shulgina, T., Clemesha, R. E. S., Guirguis, K., Pierce, D. W., Dettinger, M. D.,
 1128 Lavers, D. A., Cayan, D. R., Polade, S. D., Kalansky, J., & Ralph, F. M. (2019). Precipitation
 1129 regime change in Western North America: The role of Atmospheric Rivers. *Scientific*
 1130 *Reports*, 9(1), 9944. <https://doi.org/10.1038/s41598-019-46169-w>
- 1131 Gilbert, G. K. (1917). Hydraulic-mining Débris in the Sierra Nevada. Government Printing Office,
 1132 Department of the Interior and United States Geological Survey, Professional Paper 105.

- 1133 Gleason, K. E., Nolin, A. W., & Roth, T. R. (2013). Charred forests increase snowmelt: Effects of
 1134 burned woody debris and incoming solar radiation on snow ablation. *Geophysical*
 1135 *Research Letters*, 40(17), 4654–4661. <https://doi.org/10.1002/grl.50896>
- 1136 Goeking, S. A., & Tarboton, D. G. (2020). Forests and Water Yield: A Synthesis of Disturbance
 1137 Effects on Streamflow and Snowpack in Western Coniferous Forests. *Journal of Forestry*,
 1138 118(2), 172–192. <https://doi.org/10.1093/jofore/fvz069>
- 1139 Goeking, S. A., & Tarboton, D. G. (2022). Variable Streamflow Response to Forest Disturbance in
 1140 the Western US: A Large-Sample Hydrology Approach. *Water Resources Research*, 58(6),
 1141 e2021WR031575. <https://doi.org/10.1029/2021WR031575>
- 1142 Goss, M., Swain, D. L., Abatzoglou, J. T., Sarhadi, A., Kolden, C. A., Williams, A. P., &
 1143 Diffenbaugh, N. S. (2020). Climate change is increasing the likelihood of extreme autumn
 1144 wildfire conditions across California. *Environmental Research Letters*, 15(9), 094016.
 1145 <https://doi.org/10.1088/1748-9326/ab83a7>
- 1146 Guo, H., Goulden, M., Chung, M. G., Nyelele, C., Egoh, B., Keske, C., Conklin, M., & Bales, R.
 1147 (2023). Valuing the benefits of forest restoration on enhancing hydropower and water
 1148 supply in California’s Sierra Nevada. *Science of The Total Environment*, 876, 162836.
 1149 <https://doi.org/10.1016/j.scitotenv.2023.162836>
- 1150 Halofsky, J. E., Peterson, D. L., Buluç, L. Y., & Ko, J. M. (2021). Climate change vulnerability and
 1151 adaptation for infrastructure and recreation in the Sierra Nevada (PSW-GTR-272; p.
 1152 PSW-GTR-272). U.S. Department of Agriculture, Forest Service, Pacific Southwest
 1153 Research Station. <https://doi.org/10.2737/PSW-GTR-272>
- 1154 Harpold, A. A., Biederman, J. A., Condon, K., Merino, M., Korgaonkar, Y., Nan, T., Sloat, L. L.,
 1155 Ross, M., & Brooks, P. D. (2014). Changes in snow accumulation and ablation following
 1156 the Las Conchas Forest Fire, New Mexico, USA. *Ecohydrology*, 7(2), 440–452.
 1157 <https://doi.org/10.1002/eco.1363>
- 1158 Harpold, A. A., & Kohler, M. (2017). Potential for Changing Extreme Snowmelt and Rainfall
 1159 Events in the Mountains of the Western United States. *Journal of Geophysical Research:*
 1160 *Atmospheres*, 122(24), 13,219-13,228. <https://doi.org/10.1002/2017JD027704>
- 1161 Harpold, A. A., Krogh, S. A., Kohler, M., Eckberg, D., Greenberg, J., Sterle, G., & Broxton, P. D.
 1162 (2020). Increasing the efficacy of forest thinning for snow using high-resolution
 1163 modeling: A proof of concept in the Lake Tahoe Basin, California, USA. *Ecohydrology*,
 1164 13(4), e2203. <https://doi.org/10.1002/eco.2203>
- 1165 He, L., Ivanov, V. Y., Bohrer, G., Thomsen, J. E., Vogel, C. S., & Moghaddam, M. (2013). Temporal
 1166 dynamics of soil moisture in a northern temperate mixed successional forest after a
 1167 prescribed intermediate disturbance. *Agricultural and Forest Meteorology*, 180, 22–33.
 1168 <https://doi.org/10.1016/j.agrformet.2013.04.014>

- 1169 Hessburg, P. F., Miller, C. L., Parks, S. A., Povak, N. A., Taylor, A. H., Higuera, P. E., Prichard, S. J.,
 1170 North, M. P., Collins, B. M., Hurteau, M. D., Larson, A. J., Allen, C. D., Stephens, S. L.,
 1171 Rivera-Huerta, H., Stevens-Rumann, C. S., Daniels, L. D., Gedalof, Z., Gray, R. W., Kane, V.
 1172 R., ... Salter, R. B. (2019). Climate, Environment, and Disturbance History Govern
 1173 Resilience of Western North American Forests. *Frontiers in Ecology and Evolution*, 7.
 1174 <https://doi.org/10.3389/fevo.2019.00239>
- 1175 Hibbert, A. (1967). Forest treatment effects on water yield. In W. A. L. H. Sopper (Ed.),
 1176 International symposium on forest hydrology (pp. 527–543). Pergamon, Oxford.
- 1177 Hou, Z., Ren, H., Sun, N., Wigmosta, M. S., Liu, Y., Leung, L. R., Yan, H., Skaggs, R., & Coleman, A.
 1178 (2019). Incorporating Climate Nonstationarity and Snowmelt Processes in Intensity–
 1179 Duration–Frequency Analyses with Case Studies in Mountainous Areas. *Journal of*
 1180 *Hydrometeorology*, 20(12), 2331–2346. <https://doi.org/10.1175/JHM-D-19-0055.1>
- 1181 Huang, X., & Swain, D. L. (2022). Climate change is increasing the risk of a California megaflood.
 1182 *Science Advances*, 8(32), eabq0995. <https://doi.org/10.1126/sciadv.abq0995>
- 1183 Huang, X., Swain, D. L., & Hall, A. D. (2020). Future precipitation increase from very high
 1184 resolution ensemble downscaling of extreme atmospheric river storms in California.
 1185 *Science Advances*, 6(29), eaba1323. <https://doi.org/10.1126/sciadv.aba1323>
- 1186 Hungerford, R. D., Nemani, R. R., Running, S. W., & Coughlan, J. C. (1989). MTCLIM: A mountain
 1187 microclimate simulation model (INT-RP-414; p. INT-RP-414). U.S. Department of
 1188 Agriculture, Forest Service, Intermountain Forest and Range Experiment Station,
 1189 Research Paper INT-414. <https://doi.org/10.2737/INT-RP-414>
- 1190 Huning, L. S., & Margulis, S. A. (2017). Climatology of seasonal snowfall accumulation across the
 1191 Sierra Nevada (USA): Accumulation rates, distributions, and variability. *Water Resources*
 1192 *Research*, 53(7), 6033–6049. <https://doi.org/10.1002/2017WR020915>
- 1193 Jackson, R. B., Canadell, J., Ehleringer, J. R., Mooney, H. A., Sala, O. E., & Schulze, E. D. (1996). A
 1194 global analysis of root distributions for terrestrial biomes. *Oecologia*, 108(3), 389–411.
 1195 <https://doi.org/10.1007/BF00333714>
- 1196 Jones, D. R., Schonlau, M., & Welch, W. J. (1998). Efficient Global Optimization of Expensive
 1197 Black-Box Functions. *Journal of Global Optimization*, 13(4), 455–492.
 1198 <https://doi.org/10.1023/A:1008306431147>
- 1199 Jones, J. A., & Grant, G. E. (1996). Peak Flow Responses to Clear-Cutting and Roads in Small and
 1200 Large Basins, Western Cascades, Oregon. *Water Resources Research*, 32(4), 959–974.
 1201 <https://doi.org/10.1029/95WR03493>
- 1202 Kalies, E. L., & Yocom Kent, L. L. (2016). Tamm Review: Are fuel treatments effective at
 1203 achieving ecological and social objectives? A systematic review. *Forest Ecology and*
 1204 *Management*, 375, 84–95. <https://doi.org/10.1016/j.foreco.2016.05.021>

- 1205 Kattelman, R. C., Berg, N. H., & Rector, J. (1983). The Potential for Increasing Streamflow from
 1206 Sierra Nevada Watersheds. *JAWRA Journal of the American Water Resources*
 1207 *Association*, 19(3), 395–402. <https://doi.org/10.1111/j.1752-1688.1983.tb04596.x>
- 1208 Kennedy, J., & Eberhart, R. (1995). Particle swarm optimization. Proceedings of ICNN '95 -
 1209 International Conference on Neural Networks, 4, 1942–1948 vol.4.
 1210 <https://doi.org/10.1109/ICNN.1995.488968>
- 1211 King, J. G., & Tennyson, L. C. (1984). Alteration of Streamflow Characteristics Following Road
 1212 Construction in North Central Idaho. *Water Resources Research*, 20(8), 1159–1163.
 1213 <https://doi.org/10.1029/WR020i008p01159>
- 1214 Knapp, E. E., Bernal, A. A., Kane, J. M., Fettig, C. J., & North, M. P. (2021). Variable thinning and
 1215 prescribed fire influence tree mortality and growth during and after a severe drought.
 1216 *Forest Ecology and Management*, 479, 118595.
 1217 <https://doi.org/10.1016/j.foreco.2020.118595>
- 1218 Koltunov, A., Ramirez, C. M., Ustin, S. L., Slaton, M., & Haunreiter, E. (2020). eDaRT: The
 1219 Ecosystem Disturbance and Recovery Tracker system for monitoring landscape
 1220 disturbances and their cumulative effects. *Remote Sensing of Environment*, 238, 111482.
 1221 <https://doi.org/10.1016/j.rse.2019.111482>
- 1222 Lewis, G., Harpold, A., Krogh, S. A., Broxton, P., & Manley, P. N. (2023). The prediction of
 1223 uneven snowpack response to forest thinning informs forest restoration in the central
 1224 Sierra Nevada. *Ecohydrology*, 16(7), e2580. <https://doi.org/10.1002/eco.2580>
- 1225 Lewis, J., Mori, S. R., Keppeler, E. T., & Ziemer, R. R. (2001). Impacts of logging on storm peak
 1226 flows, flow volumes and suspended sediment loads in Caspar Creek, California. In: Mark
 1227 S. Wigmosta and Steven J. Burges (Eds.) *Land Use and Watersheds: Human Influence on*
 1228 *Hydrology and Geomorphology in Urban and Forest Areas*. Water Science and
 1229 Application Volume 2, American Geophysical Union, Washington, D.C.; 85-125.
 1230 <https://www.fs.usda.gov/research/treesearch/7822>
- 1231 Liang, S., Hurteau, M. D., & Westerling, A. L. (2018). Large-scale restoration increases carbon
 1232 stability under projected climate and wildfire regimes. *Frontiers in Ecology and the*
 1233 *Environment*, 16(4), 207–212. <https://doi.org/10.1002/fee.1791>
- 1234 Link, T. E., Unsworth, M., & Marks, D. (2004). The dynamics of rainfall interception by a
 1235 seasonal temperate rainforest. *Agricultural and Forest Meteorology*, 124(3), 171–191.
 1236 <https://doi.org/10.1016/j.agrformet.2004.01.010>
- 1237 Loudermilk, E. L., Scheller, R. M., Weisberg, P. J., & Kretchun, A. (2017). Bending the carbon
 1238 curve: Fire management for carbon resilience under climate change. *Landscape Ecology*,
 1239 32(7), 1461–1472. <https://doi.org/10.1007/s10980-016-0447-x>

- 1240 Ma, S., Concilio, A., Oakley, B., North, M., & Chen, J. (2010). Spatial variability in microclimate in
 1241 a mixed-conifer forest before and after thinning and burning treatments. *Forest Ecology*
 1242 *and Management*, 259(5), 904–915. <https://doi.org/10.1016/j.foreco.2009.11.030>
- 1243 Manley, P. N., Povak, N. A., Wilson, K. N., Fairweather, M. L., Griffey, V., & Long, L. L. (2023).
 1244 Blueprint for resilience: The Tahoe-Central Sierra Initiative (PSW-GTR-277; p. PSW-GTR-
 1245 277). U.S. Department of Agriculture, Forest Service, Pacific Southwest Research Station.
 1246 <https://doi.org/10.2737/PSW-GTR-277>
- 1247 Margulis, S. A., Cortés, G., Giroto, M., & Durand, M. (2016). A Landsat-Era Sierra Nevada Snow
 1248 Reanalysis (1985–2015). *Journal of Hydrometeorology*, 17(4), 1203–1221.
 1249 <https://doi.org/10.1175/JHM-D-15-0177.1>
- 1250 Marlon, J. R., Bartlein, P. J., Gavin, D. G., Long, C. J., Anderson, R. S., Briles, C. E., Brown, K. J.,
 1251 Colombaroli, D., Hallett, D. J., Power, M. J., Scharf, E. A., & Walsh, M. K. (2012). Long-
 1252 term perspective on wildfires in the western USA. *Proceedings of the National Academy*
 1253 *of Sciences*, 109(9), E535–E543. <https://doi.org/10.1073/pnas.1112839109>
- 1254 Martin, K. A., Van Stan II, J. T., Dickerson-Lange, S. E., Lutz, J. A., Berman, J. W., Gersonde, R., &
 1255 Lundquist, J. D. (2013). Development and testing of a snow interceptometer to quantify
 1256 canopy water storage and interception processes in the rain/snow transition zone of the
 1257 North Cascades, Washington, USA. *Water Resources Research*, 49(6), 3243–3256.
 1258 <https://doi.org/10.1002/wrcr.20271>
- 1259 Maxwell, C. J., Scheller, R. M., Wilson, K. N., & Manley, P. N. (2022). Assessing the effectiveness
 1260 of landscape-scale forest adaptation actions to improve resilience under projected
 1261 climate change. *Frontiers in Forests and Global Change*, 5.
 1262 <https://www.frontiersin.org/articles/10.3389/ffgc.2022.740869>
- 1263 Meili, N., Beringer, J., Zhao, J., & Fatichi, S. (2024). Aerodynamic effects cause higher forest
 1264 evapotranspiration and water yield reductions after wildfires in tall forests. *Global*
 1265 *Change Biology*, 30(1), e16995. <https://doi.org/10.1111/gcb.16995>
- 1266 Mijic, A., Liu, L., O’Keeffe, J., Dobson, B., & Chun, K. P. (2023). A meta-model of socio-
 1267 hydrological phenomena for sustainable water management. *Nature Sustainability*, 7(1),
 1268 7–14. <https://doi.org/10.1038/s41893-023-01240-3>
- 1269 Moore, G. W., & Heilman, J. L. (2011). Proposed principles governing how vegetation changes
 1270 affect transpiration. *Ecohydrology*, 4(3), 351–358. <https://doi.org/10.1002/eco.232>
- 1271 Moore, R., & Wondzell, S. M. (2005). Physical Hydrology and the Effects of Forest Harvesting in
 1272 the Pacific Northwest: A Review. *JAWRA Journal of the American Water Resources*
 1273 *Association*, 41(4), 763–784. <https://doi.org/10.1111/j.1752-1688.2005.tb04463.x>

- 1274 Morecroft, M. D., Taylor, M. E., & Oliver, H. R. (1998). Air and soil microclimates of deciduous
 1275 woodland compared to an open site. *Agricultural and Forest Meteorology*, 90(1), 141–
 1276 156. [https://doi.org/10.1016/S0168-1923\(97\)00070-1](https://doi.org/10.1016/S0168-1923(97)00070-1)
- 1277 Morris, M. D., & Mitchell, T. J. (1995). Exploratory designs for computational experiments.
 1278 *Journal of Statistical Planning and Inference*, 43(3), 381–402.
 1279 [https://doi.org/10.1016/0378-3758\(94\)00035-T](https://doi.org/10.1016/0378-3758(94)00035-T)
- 1280 National Interagency Fire Center. (2019). Historic Fire Perimeters [Dataset]. [https://data-](https://data-nifc.opendata.arcgis.com/search?tags=fire_progression_opendata%2CCategory)
 1281 [nifc.opendata.arcgis.com/search?tags=fire_progression_opendata%2CCategory](https://data-nifc.opendata.arcgis.com/search?tags=fire_progression_opendata%2CCategory)
- 1282 North, M., Innes, J., & Zald, H. (2007). Comparison of thinning and prescribed fire restoration
 1283 treatments to Sierran mixed-conifer historic conditions. *Canadian Journal of Forest*
 1284 *Research*, 37(2), 331–342. <https://doi.org/10.1139/X06-236>
- 1285 Patton, N. R., Lohse, K. A., Godsey, S. E., Crosby, B. T., & Seyfried, M. S. (2018). Predicting soil
 1286 thickness on soil mantled hillslopes. *Nature Communications*, 9(1), Article 1.
 1287 <https://doi.org/10.1038/s41467-018-05743-y>
- 1288 Perry, T. D., & Jones, J. A. (2017). Summer streamflow deficits from regenerating Douglas-fir
 1289 forest in the Pacific Northwest, USA. *Ecohydrology*, 10(2), e1790.
 1290 <https://doi.org/10.1002/eco.1790>
- 1291 Pomeroy, J., Fang, X., & Ellis, C. (2012). Sensitivity of snowmelt hydrology in Marmot Creek,
 1292 Alberta, to forest cover disturbance. *Hydrological Processes*, 26(12), 1891–1904.
 1293 <https://doi.org/10.1002/hyp.9248>
- 1294 PRISM Climate Group. (2022). PRISM Gridded Climate Data, 800 m Normals [Dataset]. Oregon
 1295 State University. <https://prism.oregonstate.edu>
- 1296 Quesnel Seipp, K., Maurer, T., Elias, M., Saksa, P., Keske, C., Oleson, K., Egoh, B., Cleveland, R.,
 1297 Nyelele, C., Goncalves, N., Hemes, K., Wyrsh, P., Lewis, D., Chung, M. G., Guo, H.,
 1298 Conklin, M., & Bales, R. (2023). A multi-benefit framework for funding forest
 1299 management in fire-driven ecosystems across the Western U.S. *Journal of*
 1300 *Environmental Management*, 344, 118270.
 1301 <https://doi.org/10.1016/j.jenvman.2023.118270>
- 1302 Rambo, T. R., & North, M. P. (2009). Canopy microclimate response to pattern and density of
 1303 thinning in a Sierra Nevada forest. *Forest Ecology and Management*, 257(2), 435–442.
 1304 <https://doi.org/10.1016/j.foreco.2008.09.029>
- 1305 Rasmussen, C. E., & Williams, C. K. I. (2008). *Gaussian Processes for Machine Learning*. MIT
 1306 Press.

- 1307 Roche, J. W., Goulden, M. L., & Bales, R. C. (2018). Estimating evapotranspiration change due to
 1308 forest treatment and fire at the basin scale in the Sierra Nevada, California.
 1309 *Ecohydrology*, 11(7), e1978. <https://doi.org/10.1002/eco.1978>
- 1310 Roche, J. W., Ma, Q., Rungee, J., & Bales, R. C. (2020). Evapotranspiration Mapping for Forest
 1311 Management in California's Sierra Nevada. *Frontiers in Forests and Global Change*, 3.
 1312 <https://doi.org/10.3389/ffgc.2020.00069>
- 1313 Roustant, O., Ginsbourger, D., & Deville, Y. (2012). DiceKriging, DiceOptim: Two R Packages for
 1314 the Analysis of Computer Experiments by Kriging-Based Metamodeling and
 1315 Optimization. *Journal of Statistical Software*, 51, 1–55.
 1316 <https://doi.org/10.18637/jss.v051.i01>
- 1317 Safford, H. D., Paulson, A. K., Steel, Z. L., Young, D. J. N., & Wayman, R. B. (2022). The 2020
 1318 California fire season: A year like no other, a return to the past or a harbinger of the
 1319 future? *Global Ecology and Biogeography*, 31(10), 2005–2025.
 1320 <https://doi.org/10.1111/geb.13498>
- 1321 Saksa, P. C., Bales, R. C., Tague, C. L., Battles, J. J., Tobin, B. W., & Conklin, M. h. (2020). Fuels
 1322 treatment and wildfire effects on runoff from Sierra Nevada mixed-conifer forests.
 1323 *Ecohydrology*, 13(3), e2151. <https://doi.org/10.1002/eco.2151>
- 1324 Saksa, P. C., Conklin, M. H., Battles, J. J., Tague, C. L., & Bales, R. C. (2017). Forest thinning
 1325 impacts on the water balance of Sierra Nevada mixed-conifer headwater basins. *Water*
 1326 *Resources Research*, 53(7), 5364–5381. <https://doi.org/10.1002/2016WR019240>
- 1327 Scheller, R., Kretchun, A., Hawbaker, T. J., & Henne, P. D. (2019). A landscape model of variable
 1328 social-ecological fire regimes. *Ecological Modelling*, 401, 85–93.
 1329 <https://doi.org/10.1016/j.ecolmodel.2019.03.022>
- 1330 Scheller, R. M., Domingo, J. B., Sturtevant, B. R., Williams, J. S., Rudy, A., Gustafson, E. J., &
 1331 Mladenoff, D. J. (2007). Design, development, and application of LANDIS-II, a spatial
 1332 landscape simulation model with flexible temporal and spatial resolution. *Ecological*
 1333 *Modelling*, 201(3–4), 409–419. <https://doi.org/10.1016/j.ecolmodel.2006.10.009>
- 1334 Scheller, R. M., Hua, D., Bolstad, P. V., Birdsey, R. A., & Mladenoff, D. J. (2011). The effects of
 1335 forest harvest intensity in combination with wind disturbance on carbon dynamics in
 1336 Lake States Mesic Forests. *Ecological Modelling*, 222(1), 144–153.
 1337 <https://doi.org/10.1016/j.ecolmodel.2010.09.009>
- 1338 Scheller, R. M., Kretchun, A. M., Loudermilk, E. L., Hurteau, M. D., Weisberg, P. J., & Skinner, C.
 1339 (2018). Interactions Among Fuel Management, Species Composition, Bark Beetles, and
 1340 Climate Change and the Potential Effects on Forests of the Lake Tahoe Basin.
 1341 *Ecosystems*, 21(4), 643–656. <https://doi.org/10.1007/s10021-017-0175-3>

- 1342 Schoennagel, T., Balch, J. K., Brenkert-Smith, H., Dennison, P. E., Harvey, B. J., Krawchuk, M. A.,
 1343 Mietkiewicz, N., Morgan, P., Moritz, M. A., Rasker, R., Turner, M. G., & Whitlock, C.
 1344 (2017). Adapt to more wildfire in western North American forests as climate changes.
 1345 *Proceedings of the National Academy of Sciences*, 114(18), 4582–4590.
 1346 <https://doi.org/10.1073/pnas.1617464114>
- 1347 Scholl, A. E., & Taylor, A. H. (2010). Fire regimes, forest change, and self-organization in an old-
 1348 growth mixed-conifer forest, Yosemite National Park, USA. *Ecological Applications*,
 1349 20(2), 362–380. <https://doi.org/10.1890/08-2324.1>
- 1350 Schwalm, C. R., Glendon, S., & Duffy, P. B. (2020). RCP8.5 tracks cumulative CO₂ emissions.
 1351 *Proceedings of the National Academy of Sciences*, 117(33), 19656–19657.
 1352 <https://doi.org/10.1073/pnas.2007117117>
- 1353 Seidl, R., Thom, D., Kautz, M., Martin-Benito, D., Peltoniemi, M., Vacchiano, G., Wild, J., Ascoli,
 1354 D., Petr, M., Honkaniemi, J., Lexer, M. J., Trotsiuk, V., Mairota, P., Svoboda, M., Fabrika,
 1355 M., Nagel, T. A., & Reyer, C. P. O. (2017). Forest disturbances under climate change.
 1356 *Nature Climate Change*, 7(6), 395–402. <https://doi.org/10.1038/nclimate3303>
- 1357 Sen, P. K. (1968). Estimates of the Regression Coefficient Based on Kendall's Tau. *Journal of the*
 1358 *American Statistical Association*, 63(324), 1379–1389.
 1359 <https://doi.org/10.1080/01621459.1968.10480934>
- 1360 Short, K. C. (2021). Spatial wildfire occurrence data for the United States, 1992-2018
 1361 [FPA_FOD_20210617] (5th Edition) [Dataset]. <https://doi.org/10.2737/RDS-2013-0009.5>
- 1362 Skinner, C. N., & Chang, C. (1996). Fire regimes, past and present. In: Sierra Nevada Ecosystem
 1363 Project: Final Report to Congress. Vol. II. Assessments and Scientific Basis for
 1364 Management Options. Wildland Resources Center Report No. 37. Centers for Water and
 1365 Wildland Resources, University of California, Davis. 1041-1069, 2, 1041–1069.
- 1366 Soil Survey Staff. (2022). Soil Survey Geographic (SSURGO) Database [Dataset]. Natural
 1367 Resources Conservation Service, United States Department of Agriculture.
 1368 <https://sdmdataaccess.sc.egov.usda.gov>
- 1369 Startsev, A. D., & McNabb, D. H. (2000). Effects of skidding on forest soil infiltration in west-
 1370 central Alberta. *Canadian Journal of Soil Science*, 80(4), 617–624.
 1371 <https://doi.org/10.4141/S99-092>
- 1372 Steel, Z. L., Safford, H. D., & Viers, J. H. (2015). The fire frequency-severity relationship and the
 1373 legacy of fire suppression in California forests. *Ecosphere*, 6(1), art8.
 1374 <https://doi.org/10.1890/ES14-00224.1>
- 1375 Stephens, S. L., Battaglia, M. A., Churchill, D. J., Collins, B. M., Coppoletta, M., Hoffman, C. M.,
 1376 Lydersen, J. M., North, M. P., Parsons, R. A., Ritter, S. M., & Stevens, J. T. (2021). Forest

- 1377 Restoration and Fuels Reduction: Convergent or Divergent? *BioScience*, 71(1), 85–101.
1378 <https://doi.org/10.1093/biosci/biaa134>
- 1379 Stephens, S. L., Collins, B. M., Biber, E., & Fulé, P. Z. (2016). U.S. federal fire and forest policy:
1380 Emphasizing resilience in dry forests. *Ecosphere*, 7(11), e01584.
1381 <https://doi.org/10.1002/ecs2.1584>
- 1382 Stephens, S. L., Thompson, S., Boisramé, G., Collins, B. M., Ponisio, L. C., Rakhmatulina, E., Steel,
1383 Z. L., Stevens, J. T., Wagtendonk, J. W. van, & Wilkin, K. (2021). Fire, water, and
1384 biodiversity in the Sierra Nevada: A possible triple win. *Environmental Research*
1385 *Communications*, 3(8), 081004. <https://doi.org/10.1088/2515-7620/ac17e2>
- 1386 Stevens, J. T. (2017). Scale-dependent effects of post-fire canopy cover on snowpack depth in
1387 montane coniferous forests. *Ecological Applications*, 27(6), 1888–1900.
1388 <https://doi.org/10.1002/eap.1575>
- 1389 Storck, P. (2000). Trees, snow and flooding: An investigation of forest canopy effects on snow
1390 accumulation and melt at the plot and watershed scales in the Pacific Northwest
1391 (Technical Report No. 161; Water Resources Series). Department of Civil and
1392 Environmental Engineering, University of Washington.
- 1393 Storck, P., Lettenmaier, D. P., & Bolton, S. M. (2002). Measurement of snow interception and
1394 canopy effects on snow accumulation and melt in a mountainous maritime climate,
1395 Oregon, United States. *Water Resources Research*, 38(11).
1396 <https://doi.org/10.1029/2002WR001281>
- 1397 Sturtevant, B. R., Gustafson, E. J., Li, W., & He, H. S. (2004). Modeling biological disturbances in
1398 LANDIS: A module description and demonstration using spruce budworm. *Ecological*
1399 *Modelling*, 180(1), 153–174. <https://doi.org/10.1016/j.ecolmodel.2004.01.021>
- 1400 Sun, N., Wigmosta, M., Zhou, T., Lundquist, J., Dickerson-Lange, S., & Cristea, N. (2018).
1401 Evaluating the functionality and streamflow impacts of explicitly modelling forest–snow
1402 interactions and canopy gaps in a distributed hydrologic model. *Hydrological Processes*,
1403 32(13), 2128–2140. <https://doi.org/10.1002/hyp.13150>
- 1404 Sun, N., Yan, H., Wigmosta, M. S., Leung, L. R., Skaggs, R., & Hou, Z. (2019). Regional Snow
1405 Parameters Estimation for Large-Domain Hydrological Applications in the Western
1406 United States. *Journal of Geophysical Research: Atmospheres*, 124(10), 5296–5313.
1407 <https://doi.org/10.1029/2018JD030140>
- 1408 Swezy, C., Bailey, J., & Chung, W. (2021). Linking Federal Forest Restoration with Wood
1409 Utilization: Modeling Biomass Prices and Analyzing Forest Restoration Costs in the
1410 Northern Sierra Nevada. *Energies*, 14(9), Article 9. <https://doi.org/10.3390/en14092696>

- 1411 Tague, C., & Dugger, A. L. (2010). Ecohydrology and Climate Change in the Mountains of the
 1412 Western USA – A Review of Research and Opportunities. *Geography Compass*, 4(11),
 1413 1648–1663. <https://doi.org/10.1111/j.1749-8198.2010.00400.x>
- 1414 Taylor, A. H., Vandervlugt, A. M., Maxwell, R. S., Beaty, R. M., Airey, C., & Skinner, C. N. (2014).
 1415 Changes in forest structure, fuels and potential fire behaviour since 1873 in the Lake
 1416 Tahoe Basin, USA. *Applied Vegetation Science*, 17(1), 17–31.
 1417 <https://doi.org/10.1111/avsc.12049>
- 1418 Tennant, C. J., Harpold, A. A., Lohse, K. A., Godsey, S. E., Crosby, B. T., Larsen, L. G., Brooks, P.
 1419 D., Van Kirk, R. W., & Glenn, N. F. (2017). Regional sensitivities of seasonal snowpack to
 1420 elevation, aspect, and vegetation cover in western North America. *Water Resources*
 1421 *Research*, 53(8), 6908–6926. <https://doi.org/10.1002/2016WR019374>
- 1422 Thomas, R. B., & Megahan, W. F. (1998). Peak flow responses to clear-cutting and roads in small
 1423 and large basins, Western Cascades, Oregon: A second opinion. *Water Resources*
 1424 *Research*, 34(12), 3393–3403. <https://doi.org/10.1029/98WR02500>
- 1425 Troendle, C. A. (1979). Effect of timber harvest on water yield and timing of runoff—Snow
 1426 region. U.S. Department of Agriculture Forest Service Pacific Northwest Forest and
 1427 Range Experiment Station. <http://archive.org/details/CAT83778580>
- 1428 Troendle, C. A. (1983). The Potential for Water Yield Augmentation from Forest Management in
 1429 the Rocky Mountain Region. *JAWRA Journal of the American Water Resources*
 1430 *Association*, 19(3), 359–373. <https://doi.org/10.1111/j.1752-1688.1983.tb04593.x>
- 1431 Troendle, C. A., & King, R. M. (1985). The Effect of Timber Harvest on the Fool Creek Watershed,
 1432 30 Years Later. *Water Resources Research*, 21(12), 1915–1922.
 1433 <https://doi.org/10.1029/WR021i012p01915>
- 1434 U.S. Department of the Interior, Geological Survey, and U.S. Department of Agriculture. (2016).
 1435 LANDFIRE dataset [Dataset]. <http://www.landfire/viewer>
- 1436 U.S. Geological Survey. (2019). National Hydrography Dataset [Dataset].
 1437 <https://www.usgs.gov/national-hydrography/access-national-hydrography-products>
- 1438 U.S. Geological Survey. (2022). National Water Information System daily streamflow data for
 1439 sites 103366092, 10336610, 10336645, 10336660, 10336676, 10336730, 10336780,
 1440 10343500, 11413000, 11413300, 11427000, 11427700 [Dataset].
 1441 <http://waterdata.usgs.gov/nwis/>
- 1442 van Wagtendonk, J. W., Fites-Kaufman, J. A., Safford, H. D., North, M. P., & Collins, B. M. (2018).
 1443 Sierra Nevada Bioregion. In J. W. van Wagtendonk, N. G. Sugihara, S. L. Stephens, A. E.
 1444 Thode, K. E. Shaffer, & J. A. Fites-Kaufman (Eds.), *Fire in California's Ecosystems* (pp.
 1445 249–278). University of California Press.
 1446 <https://doi.org/10.1525/california/9780520246058.003.0012>

- 1447 Varhola, A., Coops, N. C., Weiler, M., & Moore, R. D. (2010). Forest canopy effects on snow
 1448 accumulation and ablation: An integrative review of empirical results. *Journal of*
 1449 *Hydrology*, 392(3), 219–233. <https://doi.org/10.1016/j.jhydrol.2010.08.009>
- 1450 Vogel, R. M., & Fennessey, N. M. (1995). Flow Duration Curves II: A Review of Applications in
 1451 Water Resources Planning. *JAWRA Journal of the American Water Resources*
 1452 *Association*, 31(6), 1029–1039. <https://doi.org/10.1111/j.1752-1688.1995.tb03419.x>
- 1453 Voldoire, A., Sanchez-Gomez, E., Salas y Mélia, D., Decharme, B., Cassou, C., Sénési, S., Valcke,
 1454 S., Beau, I., Alias, A., Chevallier, M., Déqué, M., Deshayes, J., Douville, H., Fernandez, E.,
 1455 Madec, G., Maisonnave, E., Moine, M.-P., Planton, S., Saint-Martin, D., ... Chauvin, F.
 1456 (2013). The CNRM-CM5.1 global climate model: Description and basic evaluation.
 1457 *Climate Dynamics*, 40(9), 2091–2121. <https://doi.org/10.1007/s00382-011-1259-y>
- 1458 Watanabe, M., Suzuki, T., O’ishi, R., Komuro, Y., Watanabe, S., Emori, S., Takemura, T., Chikira,
 1459 M., Ogura, T., Sekiguchi, M., Takata, K., Yamazaki, D., Yokohata, T., Nozawa, T., Hasumi,
 1460 H., Tatebe, H., & Kimoto, M. (2010). Improved Climate Simulation by MIROC5: Mean
 1461 States, Variability, and Climate Sensitivity. *Journal of Climate*, 23(23), 6312–6335.
 1462 <https://doi.org/10.1175/2010JCLI3679.1>
- 1463 Wigmosta, M. S., Nijssen, B., & Storck, P. (2002). The Distributed Hydrology Soil Vegetation
 1464 Model. In V. P. Singh & D. K. Frevert (Eds.), *Mathematical Models of Small Watershed*
 1465 *Hydrology and Applications* (pp. 7–42). Water Resources Publications, LLC.
- 1466 Wigmosta, M. S., Vail, L. W., & Lettenmaier, D. P. (1994). A distributed hydrology-vegetation
 1467 model for complex terrain. *Water Resources Research*, 30(6), 1665–1679.
 1468 <https://doi.org/10.1029/94WR00436>
- 1469 Winkler, R., Boon, S., Zimonick, B., & Spittlehouse, D. (2014). Snow accumulation and ablation
 1470 response to changes in forest structure and snow surface albedo after attack by
 1471 mountain pine beetle. *Hydrological Processes*, 28(2), 197–209.
 1472 <https://doi.org/10.1002/hyp.9574>
- 1473 Yuba Water Agency. (2023). Atmospheric River Control Spillway at New Bullards Bar Dam.
 1474 <https://www.yubawater.org/252/ARC-Spillway-at-New-Bullards-Bar-Dam>
- 1475 Zambrano-Bigiarini, M., Rojas, & R. (2013). A model-independent Particle Swarm Optimisation
 1476 software for model calibration. *Environmental Modelling & Software*, 43, 5–25.
 1477 <https://doi.org/10.1016/j.envsoft.2013.01.004>
- 1478 Zeller, K. A., Povak, N. A., Manley, P., Flake, S. W., & Hefty, K. L. (2023). Managing for
 1479 biodiversity: The effects of climate, management and natural disturbance on wildlife
 1480 species richness. *Diversity and Distributions*, 29(12), 1623–1638.
 1481 <https://doi.org/10.1111/ddi.13782>
- 1482

1483 **References from the Supporting Information**

- 1484 Adler, A. (2015). lamW: Lambert-W Function (Version R package version 2.1.1) [Computer
1485 software]. <https://doi.org/10.5281/zenodo.5874874>
- 1486 Alberti, M., Weeks, R., & Coe, S. (2004). Urban Land-Cover Change Analysis in Central Puget
1487 Sound. *Photogrammetric Engineering & Remote Sensing*, 70(9), 1043–1052.
1488 <https://doi.org/10.14358/PERS.70.9.1043>
- 1489 Bieger, K., Rathjens, H., Allen, P. M., & Arnold, J. G. (2015). Development and Evaluation of
1490 Bankfull Hydraulic Geometry Relationships for the Physiographic Regions of the United
1491 States. *JAWRA Journal of the American Water Resources Association*, 51(3), 842–858.
1492 <https://doi.org/10.1111/jawr.12282>
- 1493 Brooks, R. H., and Corey, A. T. (1964). Hydraulic Properties of Porous Media and Their Relation
1494 to Drainage Design. *Transactions of the ASAE*, 7(1), 0026–0028.
1495 <https://doi.org/10.13031/2013.40684>
- 1496 Carter, G. A., Smith, W. K., & Hadley, J. L. (1988). Stomatal conductance in three conifer species
1497 at different elevations during summer in Wyoming. *Canadian Journal of Forest Research*,
1498 18(2), 242–246. <https://doi.org/10.1139/x88-035>
- 1499 Cirelli, D., Equiza, M. A., Lieffers, V. J., & Tyree, M. T. (2015). Populus species from diverse
1500 habitats maintain high night-time conductance under drought. *Tree Physiology*, tpv092.
1501 <https://doi.org/10.1093/treephys/tpv092>
- 1502 Conard, S. G., Sparks, S. R., & Regelbrugge, J. C. (1997). Comparative Plant Water Relations and
1503 Soil Water Depletion Patterns of Three Seral Shrub Species on Forest Sites in
1504 Southwestern Oregon. *Forest Science*, 43(3), 336–347.
1505 <https://doi.org/10.1093/forestscience/43.3.336>
- 1506 Corless, R. M., Gonnet, G. H., Hare, D. E. G., Jeffrey, D. J., & Knuth, D. E. (1996). On the
1507 LambertW function. *Advances in Computational Mathematics*, 5(1), 329–359.
1508 <https://doi.org/10.1007/BF02124750>
- 1509 DeLucia, E. H., & Schlesinger, W. H. (1991). Resource-Use Efficiency and Drought Tolerance In
1510 Adjacent Great Basin and Sierran Plants. *Ecology*, 72(1), 51–58.
1511 <https://doi.org/10.2307/1938901>
- 1512 Denmead, O. T., & Millar, B. D. (1976). Field Studies of the Conductance of Wheat Leaves and
1513 Transpiration. *Agronomy Journal*, 68(2), 307–311.
1514 <https://doi.org/10.2134/agronj1976.00021962006800020026x>
- 1515 Dickinson, R., Henderson-Sellers, A., & Kennedy, P. (1993). Biosphere-atmosphere Transfer
1516 Scheme (BATS) Version 1e as Coupled to the NCAR Community Climate Model (p. 3040
1517 KB) [Application/pdf]. UCAR/NCAR. <https://doi.org/10.5065/D67W6959>

- 1518 Du, E., Link, T. E., Gravelle, J. A., & Hubbard, J. A. (2014). Validation and sensitivity test of the
 1519 Distributed Hydrology Soil-Vegetation Model (DHSVM) in a forested mountain
 1520 watershed. *Hydrological Processes*, 28(26), 6196–6210.
 1521 <https://doi.org/10.1002/hyp.10110>
- 1522 Farouki, O. T. (1981). The thermal properties of soils in cold regions. *Cold Regions Science and*
 1523 *Technology*, 5(1), 67–75. [https://doi.org/10.1016/0165-232X\(81\)90041-0](https://doi.org/10.1016/0165-232X(81)90041-0)
- 1524 Fetcher, N. (1976). Patterns of Leaf Resistance to Lodgepole Pine Transpiration in Wyoming.
 1525 *Ecology*, 57(2), 339–345. <https://doi.org/10.2307/1934822>
- 1526 Hinckley, T. M., Lassoie, J. P., & Running, S. W. (1978). Temporal and Spatial Variations in the
 1527 Water Status of Forest Trees. *Forest Science*, 20.
- 1528 Hughes, T. F., Latt, C. R., Tappeiner, J. C., II, & Newton, M. (1987). Biomass and Leaf-Area
 1529 Estimates for Varnishleaf Ceanothus, Deerbrush, and Whiteleaf Manzanita. *Western*
 1530 *Journal of Applied Forestry*, 2(4), 124–128. <https://doi.org/10.1093/wjaf/2.4.124>
- 1531 Kattelmann, R. (1990). Variability of Liquid Water Content in an Alpine Snowpack. *International*
 1532 *Snow Science Workshop Proceedings*, Montana State University Library, 261–265.
 1533 <http://arc.lib.montana.edu/snow-science/item/689>
- 1534 Knapp, A. K., & Smith, W. K. (1987). Stomatal and photosynthetic responses during sun/shade
 1535 transitions in subalpine plants: Influence on water use efficiency. *Oecologia*, 74(1), 62–
 1536 67. <https://doi.org/10.1007/BF00377346>
- 1537 Knauer, J., El-Madany, T. S., Zaehle, S., & Migliavacca, M. (2018). Bigleaf—An R package for the
 1538 calculation of physical and physiological ecosystem properties from eddy covariance
 1539 data. *PLoS ONE*, 13(8), e0201114. <https://doi.org/10.1371/journal.pone.0201114>
- 1540 Koç, İ. (2019). Conifers response to water stress: physiological responses and effects on nutrient
 1541 use physiology [PhD Dissertation, Michigan State University].
 1542 <https://doi.org/doi:10.25335/qx4f-7y36>
- 1543 Kummerow, J., Krause, D., & Jow, W. (1977). Root systems of chaparral shrubs. *Oecologia*,
 1544 29(2), 163–177. <https://doi.org/10.1007/BF00345795>
- 1545 Law, B. E. (1995). Estimation of leaf area index and light intercepted by shrubs from digital
 1546 videography. *Remote Sensing of Environment*, 51(2), 276–280.
 1547 [https://doi.org/10.1016/0034-4257\(94\)00054-Q](https://doi.org/10.1016/0034-4257(94)00054-Q)
- 1548 Link, T. E., & Marks, D. (1999). Point simulation of seasonal snow cover dynamics beneath
 1549 boreal forest canopies. *Journal of Geophysical Research: Atmospheres*, 104(D22),
 1550 27841–27857. <https://doi.org/10.1029/1998JD200121>

- 1551 Mahat, V., & Tarboton, D. G. (2012). Canopy radiation transmission for an energy balance
 1552 snowmelt model: canopy radiation for snowmelt. *Water Resources Research*, 48(1).
 1553 <https://doi.org/10.1029/2011WR010438>
- 1554 Marks, D., Kimball, J., Tingey, D., & Link, T. (1998). The sensitivity of snowmelt processes to
 1555 climate conditions and forest cover during rain-on-snow: A case study of the 1996
 1556 Pacific Northwest flood. *Hydrological Processes*, 12(10–11), 1569–1587.
 1557 [https://doi.org/10.1002/\(SICI\)1099-1085\(199808/09\)12:10/11<1569::AID-
 1558 HYP682>3.0.CO;2-L](https://doi.org/10.1002/(SICI)1099-1085(199808/09)12:10/11<1569::AID-HYP682>3.0.CO;2-L)
- 1559 Martin, K. A., Van Stan II, J. T., Dickerson-Lange, S. E., Lutz, J. A., Berman, J. W., Gersonde, R., &
 1560 Lundquist, J. D. (2013). Development and testing of a snow interceptometer to quantify
 1561 canopy water storage and interception processes in the rain/snow transition zone of the
 1562 North Cascades, Washington, USA. *Water Resources Research*, 49(6), 3243–3256.
 1563 <https://doi.org/10.1002/wrcr.20271>
- 1564 Matzner, S. L., Rice, K. J., & Richards, J. H. (2003). Patterns of stomatal conductance among blue
 1565 oak (*Quercus douglasii*) size classes and populations: Implications for seedling
 1566 establishment. *Tree Physiology*, 23(11), 777–784.
 1567 <https://doi.org/10.1093/treephys/23.11.777>
- 1568 McDowell, N. G., Phillips, N., Lunch, C., Bond, B. J., & Ryan, M. G. (2002). An investigation of
 1569 hydraulic limitation and compensation in large, old Douglas-fir trees. *Tree Physiology*,
 1570 22(11), 763–774. <https://doi.org/10.1093/treephys/22.11.763>
- 1571 McMichael, C. E., Hope, A. S., Roberts, D. A., & Anaya, M. R. (2004). Post-fire recovery of leaf
 1572 area index in California chaparral: A remote sensing-chronosequence approach.
 1573 *International Journal of Remote Sensing*, 25(21), 4743–4760.
 1574 <https://doi.org/10.1080/01431160410001726067>
- 1575 Moeys, J. (2018). The soil texture wizard: R functions for plotting, classifying, transforming and
 1576 exploring soil texture data [Computer software]. [https://cran.r-
 1577 project.org/web/packages/soiltexture/vignettes/soiltexture_vignette.pdf](https://cran.r-project.org/web/packages/soiltexture/vignettes/soiltexture_vignette.pdf)
- 1578 Monson, R. K., & Grant, M. C. (1989). Experimental studies of ponderosa pine. III. Differences in
 1579 photosynthesis, stomatal conductance, and water-use efficiency between two genetic
 1580 lines. *American Journal of Botany*, 76(7), 1041–1047. [https://doi.org/10.1002/j.1537-
 1581 2197.1989.tb15085.x](https://doi.org/10.1002/j.1537-2197.1989.tb15085.x)
- 1582 Renninger, H. J., Carlo, N., Clark, K. L., & Schafer, K. V. R. (2014). Physiological strategies of co-
 1583 occurring oaks in a water- and nutrient-limited ecosystem. *Tree Physiology*, 34(2), 159–
 1584 173. <https://doi.org/10.1093/treephys/tpt122>
- 1585 Riikonen, J., Kets, K., Darbah, J., Oksanen, E., Sober, A., Vapaavuori, E., Kubiske, M. E., Nelson,
 1586 N., & Karnosky, D. F. (2008). Carbon gain and bud physiology in *Populus tremuloides* and

- 1587 *Betula papyrifera* grown under long-term exposure to elevated concentrations of CO₂
 1588 and O₃. *Tree Physiology*, 28(2), 243–254. <https://doi.org/10.1093/treephys/28.2.243>
- 1589 Rood, S. B., Bigelow, S. G., & Hall, A. A. (2011). Root architecture of riparian trees: River cut-
 1590 banks provide natural hydraulic excavation, revealing that cottonwoods are facultative
 1591 phreatophytes. *Trees*, 25(5), 907–917. <https://doi.org/10.1007/s00468-011-0565-7>
- 1592 Ross, K. M., & Loik, M. E. (2021). Photosynthetic sensitivity to historic meteorological variability
 1593 for conifers in the eastern Sierra Nevada. *International Journal of Biometeorology*, 65(6),
 1594 851–863. <https://doi.org/10.1007/s00484-020-02062-0>
- 1595 Running, S. W. (1976). Environmental control of leaf water conductance in conifers. *Canadian*
 1596 *Journal of Forest Research*, 6(1), 104–112. <https://doi.org/10.1139/x76-013>
- 1597 Sala, A., Carey, E. V., Keane, R. E., & Callaway, R. M. (2001). Water use by whitebark pine and
 1598 subalpine fir: Potential consequences of fire exclusion in the northern Rocky Mountains.
 1599 *Tree Physiology*, 21(11), 717–725. <https://doi.org/10.1093/treephys/21.11.717>
- 1600 Shuttleworth, J. W. (1993). Evaporation. In D. R. Maidment (Ed.), *Handbook of Hydrology* (pp.
 1601 98–144). McGraw-Hill.
- 1602 Steele, S. J., Gower, S. T., Vogel, J. G., & Norman, J. M. (1997). Root mass, net primary
 1603 production and turnover in aspen, jack pine and black spruce forests in Saskatchewan
 1604 and Manitoba, Canada. *Tree Physiology*, 17(8–9), 577–587.
 1605 <https://doi.org/10.1093/treephys/17.8-9.577>
- 1606 Svejcar, T., & Riegel, G. M. (1998). Spatial pattern of gas exchange for montane moist meadow
 1607 species. *Journal of Vegetation Science*, 9(1), 85–94. <https://doi.org/10.2307/3237226>
- 1608 Tan, C.-S. (1977). A Study of Stomatal Diffusion Resistance in a Douglas Fir Forest [PhD
 1609 Dissertation, The University of British Columbia]. [http://resolve.library.ubc.ca/cgi-
 1610 bin/catsearch?bid=1565303](http://resolve.library.ubc.ca/cgi-bin/catsearch?bid=1565303)
- 1611 Thyer, M., Beckers, J., Spittlehouse, D., Alila, Y., & Winkler, R. (2004). Diagnosing a distributed
 1612 hydrologic model for two high-elevation forested catchments based on detailed stand-
 1613 and basin-scale data. *Water Resources Research*, 40(1).
 1614 <https://doi.org/10.1029/2003WR002414>
- 1615 van Genuchten, M. T. (1980). A Closed-form Equation for Predicting the Hydraulic Conductivity
 1616 of Unsaturated Soils. *Soil Science Society of America Journal*, 44(5), 892–898.
 1617 <https://doi.org/10.2136/sssaj1980.03615995004400050002x>
- 1618 van Heeswijk, M., Kimball, J. S., & Marks, D. (1996). Simulation of water available for runoff in
 1619 clearcut forest openings during rain-on-snow events in the western Cascade Range of
 1620 Oregon and Washington. U.S. Geological Survey Water-Resources Investigations Report
 1621 95-4219. <https://doi.org/10.3133/wri954219>

- 1622 Wolfram Research. (1988). Solve, Wolfram Language function (Version Updated 2020)
1623 [Computer software]. <https://reference.wolfram.com/language/ref/Solve.html>
- 1624 Yoder, B. J. (1983). Comparative Water Relations of *Abies grandis*, *Abies concolor* and Their
1625 Hybrids [Masters Thesis, Oregon State University].
1626 https://ir.library.oregonstate.edu/concern/graduate_thesis_or_dissertations/wh246x36
1627 p
- 1628